https://doi.org/10.5194/egusphere-2025-6204
Preprint. Discussion started: 13 January 2026

Methane and carbon dioxide dynamics beneath the Greenland Ice Sheet: Insights from ice core basal materials

Lisa Ardoin[1], Catherine Larose[2], Jean-Louis Tison[1], Christoph Keuschnig[3], Vasileios Gkinis[4], Saïda El Amri[1], Pierre-Henry Blard[5], Paul Bierman[6,7], Thomas Blunier[4], Dorthe Dahl-Jensen[4], Charlotte Maistriau[1], Jørgen-Peder Steffensen[4], Thomas Röckmann[8], François Fripiat[1]

[1]Department of Geosciences, Environment and Society, Université Libre de Bruxelles, Brussels, Belgium
[2]University Grenoble Alpes, CNRS, INRAE, IRD, Grenoble INP, IGE, Grenoble, France
[3]Interface Geochemistry, German Research Center for Geosciences, GFZ, Postdam, Germany
[4]Centre for Ice and Climate, Niels Bohr Institute, University of Copenhagen, Copenhagen, Denmark
[5]Centre de Recherches Pétrographiques et Géochimiques, CNRS, Université de Lorraine, Nancy, France
[6]Rubenstein School of the Environment and Natural Resources, University of Vermont, Burlington, USA
[7]Gund Institute for Environment, University of Vermont, Burlington, USA
[8]Institute for Marine and Atmospheric research Utrecht, Utrecht University, Utrecht, Netherlands

Correspondence to: L. Ardoin (lisa.ardoin@ulb.be) and F. Fripiat (francois.fripiat@ulb.be)

Short summary

We investigated gas dynamic at the ice-bed interface of two Greenland ice cores to assess methane and carbon dioxide dynamics beneath ice sheets. At Camp Century, methane diffuses across the sediment-ice interface and is partly consumed to form carbon dioxide. At GRIP, methane remains preserved despite the presence of oxygen. These contrasts indicate that methane oxidation may be controlled by local bed conditions, including ice thickness, flow dynamics, and substrate availability.

Abstract. Ice sheets and their subglacial environments may represent an important source of methane (CH_4) and carbon dioxide (CO_2), potentially contributing to the atmospheric burden of these greenhouse gases. In this study, we investigate CH_4 and CO_2 production, transport, and consumption at and near the sediment-ice interface beneath the Greenland Ice Sheet, utilizing basal materials from two deep-drilling projects. At the Camp Century site, on the northwestern margin of the Greenland Ice Sheet, vertical gas profiles (N_2, O_2, Ar, CO_2, and CH_4), combined with microbial DNA analyses, indicate that CH_4 accumulates in subglacial environments either from the release of gases from buried soils and sediments beneath the ice sheet or via *in situ* methanogenesis. The CH_4 then diffuses across the sediment-ice interface and undergoes partial oxidation to CO_2 within debris-rich ice layers, contributing to the pronounced CO_2 accumulation near the interface. CH_4 and CO_2 remain at higher concentrations than atmospheric levels for several tens of meters in the upper section of the basal ice sequence, suggesting mechanical mixing possibly during advection from inland. At the GRIP site, located at the summit of the Greenland Ice Sheet, biologically derived CH_4 and CO_2 in basal materials is transported into the ice predominantly through mechanical mixing processes such as shearing and folding, although diffusion across the sediment-ice interface could also occur in the unsampled bottom section. There is no evidence of CH_4 consumption by methanotrophs at GRIP, suggesting that variations of

https://doi.org/10.5194/egusphere-2025-6204
Preprint. Discussion started: 13 January 2026

bed conditions, ice dynamics and the nature of the organic material control the fate of CH_4 produced in the subglacial environments.

1 Introduction

Large uncertainties on subglacial reservoirs of carbon cycling below ice sheets exist because of the difficulties related to directly accessing the environment. Until recently, ice sheets were not considered as contributors to the global carbon cycle as the ice cover prevents exchange with the atmosphere (Wadham et al., 2019). Recent studies have revealed that the Greenland Ice Sheet host active carbon cycling processes, including the production and emission of greenhouse gases such as CH_4 and CO_2 (Adnew et al., 2025; Burns et al., 2018; Christiansen et al., 2021; Lamarche-Gagnon et al., 2019; Pain et al., 2021; Wadham et al., 2019). The resulting emission of CH_4 (in mol m^2 d^{-1}) from subglacial runoff at the margins of the Greenland Ice Sheet are comparable to those of major world rivers (Lamarche-Gagnon et al., 2019). Nevertheless, significant uncertainties persist regarding the nature of subglacial environments, as well as the mechanisms governing the production, transport, and consumption of these greenhouse gases beneath ice sheets. The subglacial environment contains buried ecosystems and stores organic matter derived from ancient sediments, soils and vegetation (Bierman et al., 2014; Christ et al., 2021; Souchez et al., 2006; Willerslev et al., 2007). This organic material can serve as a substrates for microbial activity or release previously stored carbon-rich gases when exposed to the relatively warmer conditions at the base of ice sheets (Wadham et al., 2008; Souchez et al., 2006; Tison et al., 1998).

The discovery of microorganisms in subglacial environments confirms that glaciers and ice-sheet beds are not sterile but host a diverse and metabolically active microbial communities (Doyle et al., 2013; Sharp et al., 1999; Skidmore et al., 2005, 2000). Microbial respiration of organic matter consumes O_2 and produces CO_2 (Pain et al., 2021; Souchez et al., 2006; Tranter et al., 2002), creating anoxic conditions that are favorable for methanogenic activity and, consequently, CH_4 production and accumulation (Adnew et al., 2025; Dieser, 2014; Lamarche-Gagnon et al., 2019; Pain et al., 2021; Souchez et al., 2006; Verbeke et al., 2002; Wadham et al., 2008).

Although still subject to significant uncertainty, a substantial fraction of the CH_4 produced may be oxidized by methanotrophy, either anaerobically or aerobically, *in situ* or during its transport with subglacial runoff to the ice-sheet margins (Michaud et al., 2017; Adnew et al., 2025; Lamarche-Gagnon et al., 2019; Pain et al., 2021). In addition, subglacial chemical weathering processes also influence CO_2 and O_2 concentrations (Tranter et al., 2002), further contributing to spatial and temporal heterogeneity in the observed CO_2 saturation levels of subglacial runoff (Pain et al., 2021).

The basal ice layer of an ice sheet is largely shaped by processes occurring at the ice-bed interface and often includes debris-rich ice in direct contact with the underlying bedrock. A few deep-drilling projects beneath the Greenland Ice Sheet have

https://doi.org/10.5194/egusphere-2025-6204
Preprint. Discussion started: 13 January 2026

successfully recovered this basal interface, revealing several meters (up to 25 meters) of debris-laden ice overlying bed material (Bender et al., 2010; Christ et al., 2021; Goossens et al., 2016; Souchez et al., 1994; Verbeke et al., 2002). This debris-rich ice has been shown to contain exceptionally high concentrations of CO_2 (up to 13%) and CH_4 (up to 5000 ppmv), along with O_2 depletion (Herron et al., 1979; Souchez et al., 1995b; Verbeke et al., 2002). Sediments incorporated in the debris-rich ice preserved organic carbon from the subglacial environment (Bierman et al., 2014). These elevated CO_2 and CH_4 concentrations, together with the presence of organic carbon, suggest accumulation and preservation of greenhouse gases in the deepest ice layers, offering a rare observational window into subglacial environments.

In this study, we investigate basal materials from two deep-drilling projects: Camp Century and GRIP. Located at the northwest margin of the Greenland Ice Sheet, the Camp Century ice core captures the complete transition from debris-free bottom ice to the bed material underneath the ice sheet (Bierman et al., 2024; Hansen and Langway, 1966; Herron et al., 1979), providing a unique opportunity to study the production, transport, and consumption of greenhouse gases across the bed material-ice interface. Approximately 3.44m of bed material was recovered beneath the basal ice at Camp Century. The bed material is divided in five stratigraphic units, representing different depositional environment under ice free conditions (Bierman et al., 2024; Christ et al., 2021; Collins et al., 2024). The transition between the bed and the ice is abrupt, with sediment comprising 84 weight % of the total sample in the unit in contact with the ice (Unit 5, Bierman et al., 2024). The GRIP ice core, drilled at the summit of the Greenland Ice Sheet, did not recover bedrock, but the final 6 meters of debris-rich ice contained up to 13 % of CO_2, the highest concentration measured in any ice core to date (Souchez et al., 1995b).

In this paper, we apply a multiparametric multimethod approach to analyzing both Camp Century and GRIP ice cores, combining gas composition, ice water isotopes, and prokaryotic metagenomic analyses, to investigate the production, transport and consumption of CH_4 and CO_2 in subglacial environments. By comparing Camp Century ice core at the ice sheet margin and GRIP ice core at the summit, we assess what processes shape the formation and evolution of greenhouse gas reservoirs across the base of the Greenland Ice Sheet.

2 Materials and methods

The Camp Century ice core was completed in 1966 in northwest Greenland (77° 10' N; 61° 08' W; 1885 m above sea level (Hansen and Langway, 1966; Herron et al., 1979). The basal section of the Camp Century ice core in this study spans the last lowermost 27 meters of ice above the bed material. This section includes the transition from debris-free debris-rich basal ice (16.8 m above the sediment) and from the basal ice to the bed materials, at 1387.4 m below the surface (Bierman et al., 2024; Hansen and Langway, 1966). Luminescence dating of the uppermost sediment sample indicates it was last exposed to light 416 ± 38 ka ago, corresponding to MIS 11 interglacial period (Christ et al., 2023).

https://doi.org/10.5194/egusphere-2025-6204
Preprint. Discussion started: 13 January 2026

The GRIP ice core was drilled in 1992 at the summit of the GrIS (72° 34'N; 37° 37'W; 3238 m above sea level; Dansgaard et al., 1993). About 6 m of basal ice were recovered from the bottom of the ice core located at a depth of 3022 m below the surface. The bedrock was not reached but was expected from radar soundings to be ~ 3029 m below the ice surface (D. Dahl-Jensen, pers. com. 2024). ^{40}Ar and $^{10}Be/^{36}Cl$ dating in the basal ice of GRIP gives an average age of 970 ± 140 ka (Yau et al., 2016) and 950 ± 44 ka (Willerslev et al., 2007), respectively.

The basal borehole temperature is -13°C and -9.2°C at Camp Century and GRIP, respectively; implying cold bed conditions for both sites (MacGregor et al., 2016a).

2.1 Water isotopes measurements

Samples from 5 to 10 g of Camp Century ice were collected at intervals of 40 cm, with a refined higher sampling resolution in the lower 2 meters, where intervals were reduced to approximately 15 cm. The samples were melted at ambient temperature and filtered with 2 µm polyether sulfone filters before analyses to remove the debris. The water isotopes measurements were performed at the Centre for Ice and Climate, Niels Bohr Institute (Copenhagen, Denmark) using a cavity ring-down spectrometer Picarro L2140-i following the procedure describe by Gkinis et al., (2021). Measurements are referenced to Vienna Standard Mean Ocean Water (VSMOW) using two in-house standards waters, bracketing the sample $\delta^{18}O$ and δD values (i.e., $\delta^{18}O$ (‰) = $(^{18}O/^{16}O)_{sample}/(^{18}O/^{16}O)_{SMOW} - 1$; δD (‰) = $(D/H)_{sample}/(D/H)_{SMOW} - 1$). Standard deviation (SD) was calculated using internal standard during each batch of measurements, as well as by performing triplicate analysis for each sample. For our dataset, we report median 1 SD reproducibility of 0.04 ‰ and 0.35 ‰ for $\delta^{18}O$ and δD respectively. Data are available in Ardoin et al., (2025).

2.2 Gas analyses

Measurements of gas composition (N_2, O_2, Ar, CO_2, CH_4, N_2O) were performed on 72 samples at the Université Libre de Bruxelles (Brussels, Belgium; Table S1). Data are available at Ardoin et al., (2025). For Camp century, a total of 55 samples were measured, two of them on the bed material beneath the ice and 53 from the ice-bed interface up to 26.7 meters above the bed material. Samples were collected at intervals of approximately 40 cm, with a refined higher sampling resolution in the lower 6 m where intervals were reduced to 25 cm. Gas measurements below the ice-bed interface were conducted on ice rich lenses within Unit 2 (Bierman et al., 2024), between 1.2 and 1.75 m below the sediment-ice interface. N_2O measurements are beyond the scope of this study and will be discussed in another manuscript.

Gases from GRIP basal layers were measured on 17 samples from 6.0 to 0.5 m from the bottom of the core following the same protocol as for Camp Century (note again that the GRIP core did not reach the bed material). The measurements at GRIP complement previous measurements of N_2, O_2, CO_2, and CH_4 concentrations done by Souchez et al. (1994, 1995b, 2006).

https://doi.org/10.5194/egusphere-2025-6204
Preprint. Discussion started: 13 January 2026

Entrapped gases were extracted from the ice using a melt-refreeze method (Chappellaz et al., 1997; Flückiger et al., 2002; Landais et al., 2006). The six gas species (N_2, O_2, Ar, CO_2, CH_4, N_2O) were simultaneously measured on a custom-made system using a Thermo Scientific™ TRACE™ 1310 Gas Chromatograph with various separation columns and detectors as described below. Before analysis, we trimmed the ice surface by approximately 2 mm, and on average placed 38 ± 8 g of ice in a 198 mL glass vessel. The vessel was immersed in a -30°C ethanol bath and connected to a vacuum line to evacuate the headspace for 20 minutes (down to ~ 0.5 mbar). After removing the lab atmosphere, we melted the ice in a 60°C hot water bath for 15 to 20 minutes, then refroze it from the bottom in a -30°C cold bath for 45 to 60 minutes to accumulate the entrapped gases in the headspace (Chappellaz et al., 1997).

The gas mixture in the headspace was then expanded into the extraction line through a water trap (SS U-tube immersed in -78°C ethanol cooled with dry ice) and distributed over three sample loops. The gas mixture in each sample loop is then directed to specific detectors using air-actuated valves, with helium (He) and nitrogen (N_2) as carrier gases. We used three different detectors to measure the different gases: a thermal conductivity detector (TCD) for the major gas species (N_2, O_2, Ar), a flame ionization detector (FID) coupled with a methanizer measures for CO_2 and CH_4, and an electron capture detector (ECD) for N_2O. Gas separation occurs before reaching the detectors: CH_4 is separated at 50°C using a ShinCarbon ST, 60-80 mesh column; CO_2, converted to CH_4 by the methanizer, is separated using a Hayesep Q, 60-80 mesh column; N_2O is separated using a Hayasep Q, 80-100 mesh column; and Ar-O_2-N_2 separation occurs at 5°C on a molecular sieve 5A, 60-80 mesh column. The total gas content is calculated from the sum of the number of moles of the six gases.

Two successive injections from the same extracted air sample were analysed, with the system calibrated using a standard gas mixture (AirLiquide Belgium®), named Standard 500, of 78.4 ± 1.6 %; 20.4 ± 0.4 %; 1.1 ± 0.1 %, 0.057 ± 0.001 %, 4.1 ± 0.1 ppm for N_2, O_2, Ar, CO_2, and CH_4 respectively. Standard 500 is injected at varying pressures to bracket the sample injection pressure. Accuracy and reproducibility were assessed by measuring another standard gas mixture (AirLiquide Belgium®), called Standard 800, used as our internal standard, with a composition of 83.6 ± 1.7 %; 15.0 ± 0.3 %; 1.5 ± 0.2 %, 0.080 ± 0.002 %, 5.2 ± 0.1 ppm for N_2, O_2, Ar, CO_2, and CH_4 respectively. Standard 800 is injected before each sample.

Because of the thermal gradient along the extraction line (-30 °C at the sample vessel and 50 °C in the loops), the gas does not distribute homogeneously within the line, leading to a lower effective concentration (mol L^{-1}) in the measured section. To correct for this effect, the measurements must be divided by a correction factor (CF), estimated as 0.81 ± 0.03 or 0.72 ± 0.01, depending on the line configuration. The extraction line was modified in July 2023, and the corresponding correction factors were adjusted accordingly (0.81 before the modification and 0.72 after). This correction factor was determined by filling a known volume of the extraction line at room temperature with Standard 800 and calculating the expected numbers of injected moles using the ideal gas law ($n_{theoritical}$). The gas was then expanded through the extraction line under the same conditions as

https://doi.org/10.5194/egusphere-2025-6204
Preprint. Discussion started: 13 January 2026

for an actual sample, and the number of moles effectively measured ($n_{measured}$) was quantified. The ratio $n_{measured}/ n_{theoritical}$ provides the correction factor, allowing to account for the impact of the thermal gradient.

To evaluate the procedural blanks (n_{blank}), we produced bubble free ice (BFI) by applying the melt-refreeze method six consecutive times to about 40 g of milliQ water. During the final cycle, the headspace was checked to confirm the absence of residual gas, ensuring that the resulting ice was indeed bubble-free. For O_2, Ar and CH_4, the blanks were under the limit of detection (LOD) and were, therefore, not considered in the correction. The N_2 and CO_2 blanks were $4.10\times 10\text{-}7 \pm 3.36 \times 10^{-7}$ and $1.02 \times 10^{-8} \pm 1.14\ 10^{-8}$ mol, corresponding on average to 0.9 ± 0.7 % and 6.2 ± 6.3 % of our measurements.

For the most soluble gas species (CO_2), the wet extraction induces a bias because some of the gas remains entrapped in the refrozen ice layer (Chappellaz et al., 1997). We estimated the analytical bias (AB) by applying the extraction procedure starting with 46 ± 4 g of BFI and the Standard 800 at different pressure (from ~ 12 to 25 mbar). The number of moles of each gas species was measured before (n_{before}) and after (n_{after}) the melt-refreeze method. The ratio n_{after}/ n_{before} yielded an analytical bias of 1.06 ± 0.03, 1.06 ± 0.03, 1.05 ± 0.03, 0.86 ± 0.06 and 1.10 ± 0.04 for N_2, O_2, Ar, CO_2, and CH_4 , respectively.

A measurement of gas species i in a sample ($n^i_{measured}$) was corrected for the blank (n^i_{blank}), the correction factor (CF), and the analytical bias (AB^i) as follows:

$$n^i_{corrected} = \frac{n^i_{measured} - n^i_{blank}}{CF \cdot AB^i} \qquad (1)$$

The concentration (mol kg^{-1}) and mixing ratio (mol mol^{-1}) for each gas species were subsequently derived from these corrected values. Uncertainties were propagated using standard error-propagation formulas, explicitly accounting for the covariance between dependent variables. The median relative standard deviations for the concentration (mol kg^{-1}) are 5.9, 6.5, 6.2, 9.6, and 7.0 % for N_2, O_2, Ar, CO_2, and CH_4, respectively. The median standard deviations for the mixing ratio are 2.5%, 0.6%, 0.03%, 0.11% and 10.6 ppm for N_2, O_2, Ar, CO_2, and CH_4, respectively. These standard deviations are small relative to the measured variability (Fig. 3).

Because of concerns of the melt-refreeze method for CO_2 measurements (Bereiter et al., 2015), a dry extraction technique was additionally performed on 5 samples of 41 ± 8 g at the exact same depth as samples measured with the melt-refreeze extraction methods. For this dry extraction, the ice samples were placed in a stainless-steel cylindrical container with five stainless-steel balls. The cylinder was evacuated for 45 min and maintained at -30°C connected to the vacuum line. Crushing was done in the cold room by imparting an up-and-down motion to the vessel at 5.5 Hz for 1.5 minutes (Raynaud et al., 1982). The dry extraction is not suitable for CH_4 measurements because CH_4 is formed by metal-metal frictions (Higaki et al., 2006). Still, it is the method most accurate for CO_2 as it prevents contamination from carbonated dust particles that can dissolve when the ice

https://doi.org/10.5194/egusphere-2025-6204
Preprint. Discussion started: 13 January 2026

is melted, and prohibits dissolution and refreezing of a significant fraction of CO_2 in the melt water (Raynaud et al., 1982). Gas compositions obtained from crushing and melting–freezing extractions were compared using a Mann-Whitney rank-sum test (Mann and Whitney, 1947). No significant differences were detected (p-value ≥ 0.3 for N_2, O_2, Ar, and CO_2; Fig. 3).

2.3 Debris content

The melting-freezing solid residues of debris-rich ice were carefully preserved after the gas extraction for subsequent analysis of the debris content through weight measurement. Debris collection involved melting the samples after refreezing, decanting them, and subjecting them to two rounds of centrifugation lasting 15 min each at 4000 round per minutes. Following the removal of the supernatant, the debris was dried for 48 h at 50°C in a drying oven before being weighted. The error on the debris content of each sample considers a precision of ± 0.001 mg for the debris weight and 0.01 g for the weight of the sample before gases analyses.

2.4 DNA sequencing

2.4.1 Sample processing

Ice (n = 14) and 6 blank samples (frozen milliQ water used at ULB and laboratory milliQ water used at Institut des Géociences et de l'Environnement (IGE)) were processed in the ultra-clean ice core facilities at the IGE laboratory. Samples were left to melt at room temperature and then sequentially filtered through 0.2 µm and 0.1 µm sterilized polycarbonate filters. DNA was extracted from filters using the PowerWater extraction kit. Two large debris inclusions (> 0.5 cm in diameter), both from the debris rich-ice samples at Camp Century at the depth of 6 and 0.25 m (INC 9 and 12 respectively) from the bed-ice interface, were isolated from the samples and DNA was extracted separately using the same kit as for the ice.

2.4.2 Metagenomic library preparation

Metagenomic libraries were prepared using the Illumina DNA Prep Kit. DNA was enzymatically fragmented (37°C, 15 min), ligated with Integrated DNA Technology (IDT) for Illumina UD Indexes, and primer dimers were removed via a left-hand selection of 80 bp. Libraries were PCR-amplified (20 cycles) and purified. Fragment size distribution was validated and quantified on an Agilent 4200 Bioanalyser (High Sensitivity D1000 assay). Equimolar pooled libraries were denatured with 0.2 N NaOH, diluted to 1.8 pmol L^{-1}, and spiked with 1% PhiX control v3. Sequencing was performed on an Illumina NextSeq 1000/2000 platform using the P3 600-cycle reagent kit (2 × 300 bp paired-end configuration), generating approximately 400–500 million reads per run.

2.4.3 Sequence processing

Contamination in samples containing low biomass is of critical concern and requires careful pre-filtering and evaluation of the sequencing data (Eisenhofer et al. 2019). Raw reads were filtered against blank samples and common artefact sequences in

https://doi.org/10.5194/egusphere-2025-6204
Preprint. Discussion started: 13 January 2026

NGS runs with BBDuk (https://sourceforge.net/projects/bbmap/) using the option ref = adapters, artifacts, phix, lambda, pjet, mtst, kapa. Further quality filtering included the options k = 31, mink = 9, hdist = 1, ktrim = r, qtrim = rl, trimq = 15 and maq = 10 and subsequent mapping against the human genome (T2T-CHM13v2.0, https://hgdownload.soe.ucsc.edu/downloads.html) to clean the data from potential contamination with BBmap using options k = 14 and minid = 0.95. These filtered data have been assembled with megahit (Li et al., 2015) with -k-list 21, 27, 33, 37, 45, 51, 61, 71, 81, 91 and --min-count 1, reads mapped back to contigs with bowtie2 (Langmead and Salzberg, 2012) with the –very-sensitive flag and profiled and merged using anvi-profile and anvi-merge from the ANVI'O suite (Eren et al., 2021). Contigs potentially stemming from contaminant DNA were identified by manual inspection of mapped data with anvi-interactive by binning contigs showing a similar mapping signal in all samples. This evenness in mapping rates suggested that the amount of DNA in all samples is similar which has been treated as contamination from processing steps rather than the actual signal from the analysed microbiome. Two bins of potential contaminants were taxonomically annotated to Cutibacterium ances, a common human skin associated bacterium and Enterobacteriaceae, a family of bacteria connected to the human gut. These contigs were used as a reference in a second round of filtering with BBDuk as described above which resulted in the filtered dataset used for further analysis.

Pre-filtered reads were blasted using diamond blastx (Buchfink et al., 2015) against the annotree database (Gautam et al., 2023) and annotated using the daa-meganizer command with megan-mapping-annotree-June-2021.db as mapping file and flags --lcaAlgorithm weighted, --minPercentIdentity 0.9, --topPercent 5, --lcaCoveragePercent 75. Daa files were imported into MEGAN (Huson et al., 2016) for further analysis. Key gene sequences for enzymes related to methanogenesis and methylotrophywere identified (see supplemental information) and compiled to estimate pathway completeness in each sample. Specific marker genes and taxonomy for the associated communities were also extracted from the metagenomic data.

3 Results

3.1 Facies, ice $\delta^{18}O$ and δD, and debris content

Variations in debris content at Camp Century delineate the transitions between clear debris-free ice, basal debris-rich ice, and sediments. The first appearance of debris, located at 16.8 m above the bed material, marks the onset of the basal ice section. In this section, debris content ranges from 0.08 to 1.44 weight % with a characteristic banded dispersed facies (Hubbard et al., 2009) that progressively darkens with depth (Fig. 1 a, b, c). The thickness of the darker layers varies from 0.5 to 5 cm, with no significant trend in debris content observed throughout the basal sequence (Fig. 3e). Average ice crystal diameters show a significant abrupt change from 3.84 mm to 0.79 mm 10 meters above the bedrock, with the c-axes of the small crystals showing a preferred orientation fabrics under high shear deformation (Herron et al., 1979). The debris predominantly occurs as dispersed aggregate of silt and clay-size material (clots), with typical diameter around 1 mm. In the last 30 cm above the bedrock, both

https://doi.org/10.5194/egusphere-2025-6204
Preprint. Discussion started: 13 January 2026

the size of these aggregates (up to 1 cm) and their frequency increase, raising the debris content above 1 weight % (Fig. 3e, 2c).

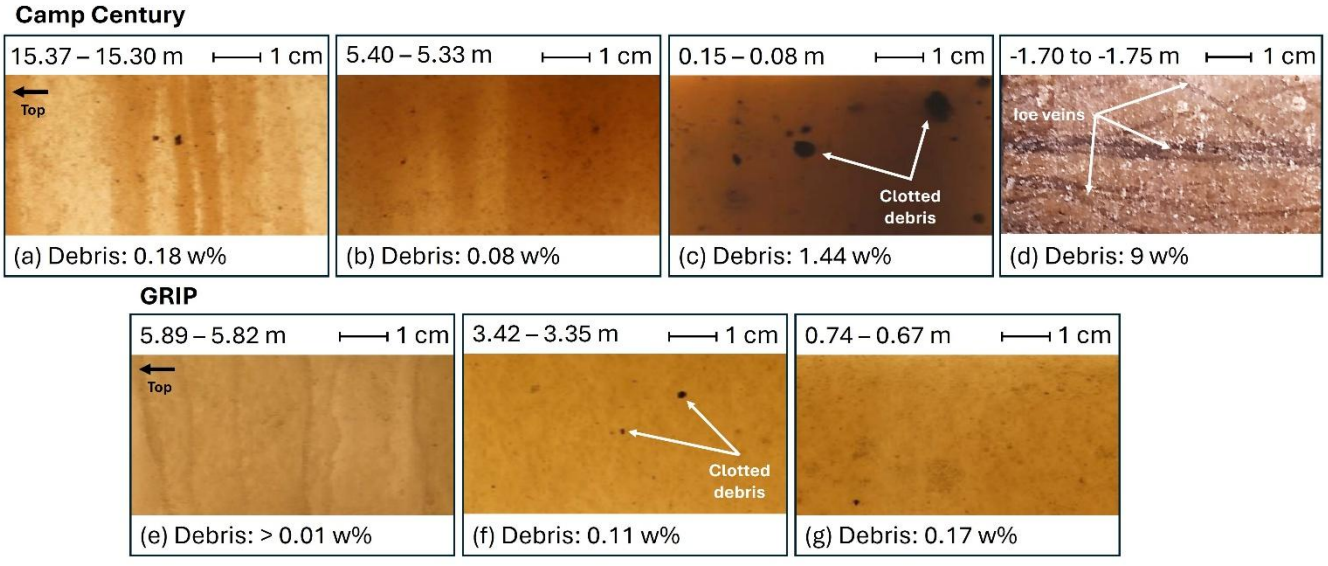

Figure 1: Representative photographs of the basal materials at Camp Century (panels a–d) and GRIP (panels e–g). For Camp Century, panels a–c are in the basal ice and panel d is the Unit 2 of the sediments (Bierman et al., 2024). "Clotted Debris" refers to debris aggregates of fine particles (Sugden et al., 1987).

A dispersed facies has been also documented in the last 6 m of the sampled GRIP ice core, with debris content measuring less than 1 % by weight (Tison et al., 1994). Like Camp Century, the debris predominantly occurs as dispersed aggregates of clotted silt and clay particles that are intermittently present throughout the sequence, with aggregate sizes varying from > 1 mm to 3 mm (Fig. 1e, f, g). The debris content gradually increases from 0.01 to 0.30 weight % with depth in the basal ice section (Fig. 3k). Our measurements and those conducted at GRIP by Souchez et al. (1995) are similar, except for a single local aggregate located at 3.04 m above the bottom of the core. Textural and crystallography investigations have identified layers up to 30 cm thick, which in some case appear to correspond to small variations (~ 0.1 % by weight) in debris content (Tison et al., 1994). In the top 1.5 m, these layers alternate large contrasts in crystal size and ice fabric (large crystals with dispersed fabric vs. small crystals with single maximum).

In the basal ice section of GRIP, ice $\delta^{18}O$ values progressively increase from -36.5 to -25.7 ‰, exceeding those of both Holocene and Eemian ice (Fig. 3h; Souchez et al., 1994). These elevated $\delta^{18}O$ values are consistent with ice formation at the ground surface in the absence of an ice sheet (i.e., at much lower elevation). This local basal ice endmember was subsequently mechanically mixed with meteoric ice and underlying sediments during the buildup of the ice sheet (Souchez et al., 2006).

https://doi.org/10.5194/egusphere-2025-6204
Preprint. Discussion started: 13 January 2026

At Camp Century, $\delta^{18}O$ depth variations oscillated between glacial and higher than Holocene values (Fig. 3b). The latter are observed in the debris-free ice at the top of the profile and in the bottom 2 m of the basal ice, while the upper layers of the debris-rich ice, above these 2 meters, exhibit lower $\delta^{18}O$ values typical of glacial periods, to a few exceptions (at 15, 11 and 8 to 9 m, Fig 3b). The top section of the debris-rich ice indeed shows a less stable profile oscillating between these two extremes.

The linear regression of δD versus $\delta^{18}O$ for both GRIP (8.01 ± 0.03; Souchez et al., 1994) and Camp Century (8.17 ± 0.04; this study) ice cores aligns with the Global Meteoritic Water line (GMWL; Fig. 2), indicating no evidence for *in-situ* refreezing at the scale of the sampling resolution (Souchez and Jouzel, 1984).

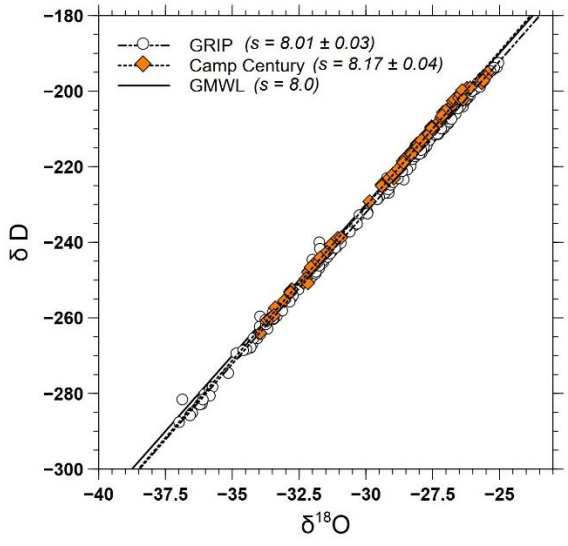

Figure 2: Relationship between ice $\delta^{18}O$ and δD in basal ice core sections from the data repository from Ardoin et al., (2025). Filled orange diamonds are for Camp Century, empty black circles for GRIP (Souchez et al., 1994). The slopes (s) are indicated in the figure caption, shown as dotted (Camp Century) and dash-dotted lines (GRIP). The Global Meteoric Water Line (GMLW) is shown as a solid black line (Craig, 1961).

3.2 Gas content and composition

Figure 3 summarizes total gas content (ml kg^{-1}) and gas mixing ratios (ppm, %) at Camp Century and GRIP. Gas concentrations (mol kg^{-1}) are given in Figure B5. Total gas content measurements align with previous studies conducted at GRIP and Camp Century (Fig. 3a, light vs. dark symbols; Herron et al., 1979; Souchez et al., 1995). At Camp Century the gas content start to decrease about 45 m above the bed materials, well above the first appearance of debris at 16.8 m above the bed where it is already down to 62.1 ± 6.2 ml kg^{-1} (Herron et al., 1979). However, the proportions of O_2, Ar, and N_2 remain consistent with atmospheric mixing ratios (Fig. 3c, f). The gas content remains relatively stable down to 3.75 meters above the bed material,

https://doi.org/10.5194/egusphere-2025-6204
Preprint. Discussion started: 13 January 2026

from 51.1 to 53.1 mL kg^{-1} with a local minimum of 33.0 mL kg^{-1} at 15.6 m above the bed, and then decreases down to 6.5 ± 0.4 ml kg^{-1} just above the bed-ice interface. The ice-rich lenses in which the gas measurements were conducted in the bed material have a slightly higher gas content of 8.4 ± 0.4 and 18.4 ± 0.9 ml kg^{-1}. At GRIP, the gas content decreases progressively from atmospheric level (84.6 ± 8.5 ml kg^{-1}) when the first debris appears at 5.98 meters from the bottom of the ice core to 72.2 ± 3.5 ml kg^{-1} at 0.76 m (this study) and 48 ml kg^{-1} at 0.35 m (Souchez et al., 1995b) within the available debris-rich section.

At Camp Century, the mixing ratios of CH_4, from 0.93 to 2.32 ppm, and CO_2, from 0.08 to 0.13 %, in the ice above the first appearance of debris exceed the glacial interglacial atmospheric range. In contrast, the mixing ratios of N_2, O_2, and Ar are indistinguishable from atmospheric levels (Fig. 3c, e, f). Similar observations are reported at GRIP. Elevated CH_4 and CO_2 levels in this ice are consistent with previous observations above debris-rich layers, suggesting microbial production through methanogenesis and respiration (Souchez et al., 1995b; Tung et al., 2006; Verbeke et al., 2002). However, these processes occur to a much lesser extent compared to debris-rich ice.

At Camp Century, the first appearance of debris is marked by a sharp decline in O_2 content from 21.4 % to 19.8 %, while other gas species show proportional increases in their mixing ratios (Fig. 1). Although the mixing ratios of N_2 and Ar (i.e. their relative fractions) increase correspondingly, their absolute bulk concentrations (in mol kg^{-1}) decrease due to the overall reduction in gas content, while CH_4 and CO_2 concentrations increase (Fig. B5). Contrasting trends are observed with depth in the basal ice section, i.e., from the first appearance of debris down to the bed material. The O_2 content continues to decrease, reaching 10 % two meters above the bed and down to 0.31 ± 0.7 % in the bed material, indicating nearly depleted O_2 conditions.

In contrast, the CO_2 mixing ratio show a peak at 11.4 ± 1.12 % at 0.8 m above the bed before decreasing down to 0.66 ± 0.11 % in the bed material. This accumulation of CO_2 just above the sediment-ice interface is also evident in the bulk concentrations (Fig. B5). The CH_4 mixing ratio irregularly increases from 8 ± 1 to 189 ± 13 ppm from the first appearance of debris to ~ 1 m above the sediments, with intermediate maxima between 355 ± 20 and 341 ± 18 ppm. Below 1 m above the sediments, CH_4 mixing ratio increases sharply up to 40 794 ± 2 217 ppm at the sediment-ice interface and in the sediments, which also corresponds to a sharp increase in bulk CH_4 concentrations despite the decreasing total gas content (Fig. B5). Ar and N_2 mixing ratios remain relatively stable or slightly increase until approximately 2 m above the bed material, where both gradually increase approaching the bed-basal ice interface, reaching 1.45 ± 0.05% and 87.3 ± 3.0 %, respectively, for the one before the last sample. This however corresponds to a clear decrease in bulk concentration for both gases (Fig. B5). In the bottom-most basal ice sample and the bed material, a decoupling between Ar and N_2 mixing ratios is observed: Ar mixing ratio decrease from 1.30 ± 0.04% to 0.69 ± 0.03%, while N_2 mixing ratio increase from 92.3 ± 2.7% to 94.6 ± 2.7%.

For GRIP, similar trends to previous measurements (Souchez et al., 1995b, a) are observed (Fig. 3g to l; Mann–Whitney rank-sum test, $p \geq 0.30$ for O_2, Ar, CO_2), confirming the long-term preservation of gases over decades of storage. As the debris

https://doi.org/10.5194/egusphere-2025-6204
Preprint. Discussion started: 13 January 2026

content increases with depth, O_2 decreases progressively from 19.7 ± 0.8 % to 2.2 ± 0.1 while CO_2 and CH_4 rise proportionally, with CO_2 increasing from 0.9 % to 15.4 % and CH_4 from 181 ppm to 4574 ppm. Although CO_2 and CH_4 mixing ratios increase markedly with depth at GRIP, their absolute bulk concentrations remain far lower than at Camp Century, with GRIP CO_2 ranging from 1.34×10^{-5} to 2.94×10^{-4} mol kg^{-1} and CH_4 from 2.35×10^{-7} to 9.00×10^{-6} mol kg^{-1}, compared with Camp Century values rising from 1.20×10^{-6} mol kg^{-1} to 1.42×10^{-4} for CO_2 and from 2.08×10^{-9} to 1.60×10^{-5} mol kg^{-1} for CH_4 (Fig. B5). The N_2 mixing ratio increases from 78.5 % to 82.9 %, whereas the Ar mixing ratio remains relatively stable at 0.98 ± 0.03 %. N_2, O_2 and Ar bulk concentrations (mol kg^{-1}) decrease systematically with depth, consistent with the progressive reduction in total gas content as debris content increases (Fig. B5).

While GRIP shows a gradual increase of both CO_2 and CH_4 mixing ratios downward within the debris-rich ice (Fig. 3i, j), Camp Century displays a decoupling between CO_2 and CH_4 maxima (Fig. 4; within the lower 2 meters above the sediment). The highest CO_2 concentrations at Camp Century are found at 0.8 meters above the bed material-ice interface, with concentrations decreasing both above and below this point (Fig. 4c). In contrast, the highest CH_4 concentrations at Camp Century are found within the bed material and just above the bed-ice interface (Fig. 4c). These concentrations drop sharply within the first meter above the bed, followed by a more gradual decline with increasing distance from the interface.

https://doi.org/10.5194/egusphere-2025-6204
Preprint. Discussion started: 13 January 2026

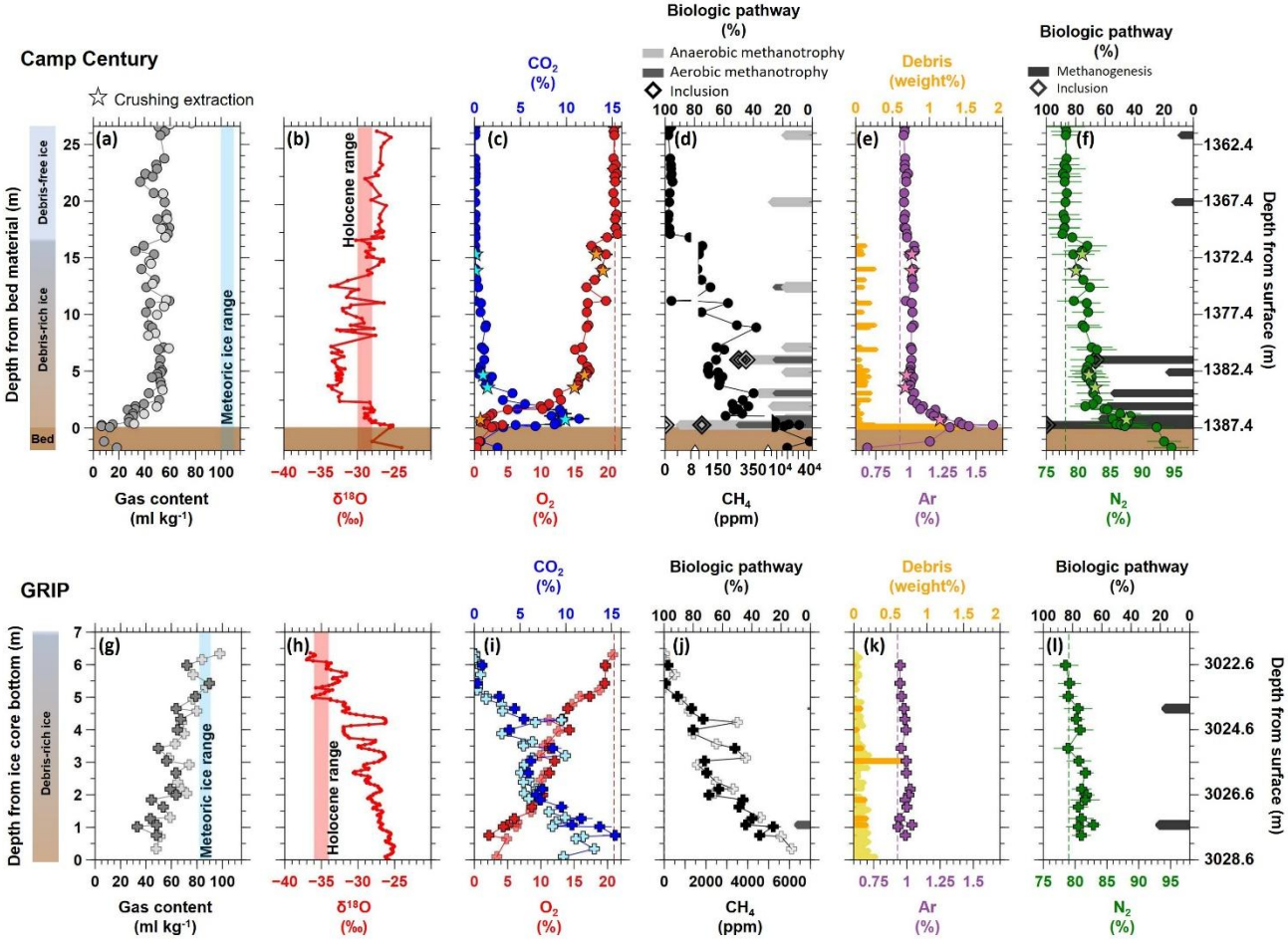

Figure 3: Gas content (a, g), ice $\delta^{18}O$ (b, h), CO_2 (blue) and O_2 (red) (c, i), CH_4 (d, j), Ar (purple) and debris content (yellow) (e, k), and N_2 (f, l) for Camp Century and GRIP, respectively. Completeness of biological pathways (see text for details) are indicated in % for CH_4 production (i.e., methanogenesis; f, i), and CH_4 consumption (i.e., methanotrophy; d, j). Lighter symbols/bars for gas content, O_2, CO_2, CH_4 and debris content are from previous studies (Herron et al., 1979; Souchez et al., 1994, 1995). Star symbols are measurements done with a dry extraction method (see section 2.1). Vertical dotted lines are the present-day atmosphere. Red shaded areas in panels (b, h) indicate the Holocene range for ice $\delta^{18}O$. Blue shaded areas in panels (a, g) are the total gas content ranges for ice formed at the present-day ice sheet altitude.

3.3 Microbial DNA sequencing

We evaluated pathway completeness by detecting essential genes for each pathway in the metagenomes. Specifically, we measured the completeness of each metabolic pathway as the fraction of necessary genes encoding the key enzymes in these processes for methanogenesis and methanotrophy (% of biological pathway in fig. 1d, j). We also identified the main microbial taxa associated with these pathways (Fig. A1).

https://doi.org/10.5194/egusphere-2025-6204
Preprint. Discussion started: 13 January 2026

In the basal ice at Camp Century, methanogenesis pathway completeness increased with depth (Figs. 3f; Table A1). Hits to genes for all three methanogenesis pathways (hydrogenotrophic, acetoclastic, and methylotrophic) were only observed in the deepest samples analyzed for microbial DNA sequencing, i.e., 0.25 m above the bed-ice interface.

Genes associated with methanotrophy were predominantly detected within the lowest 7 m of debris-rich ice at Camp Century. Pathway completeness ranged from 18 % to 100 % for anaerobic methanotrophy, and from 0% to 75% for aerobic methanotrophy (Fig. 1d, f), with the deepest samples again showing the highest levels of completeness. Based on pathway completeness, gene presence, taxonomic affiliations, and the potential for microbial consortia, the deepest Camp Century sample represents the strongest candidate for active anaerobic methanotrophy. In contrast, evidence for aerobic methanotrophy remains limited (Appendix A). The inclusions showed the highest potential for methanotrophy (Table A1). It is therefore likely that broader sampling of such inclusions would reveal higher methanotrophic potential.

The two samples analysed from the GRIP basal ice sequence show limited potential for methanogenesis and methanotrophy, with these two pathways reaching no more than 20% completeness (Fig. 1 j, l; Table A1).

4 Discussion

4.1 Methane and carbon dioxide accumulation at the ice-bed interface

We report substantial CH_4 and CO_2 accumulation in debris-rich ice of both Camp Century (up to 31 340 ppm and 9.4%, respectively) and GRIP (up to 6 100 ppm and 14.3%, respectively; Fig. 3), reaching concentrations 2 to 3 orders of magnitude higher than those in the present-day atmosphere. Similar enrichments have previously been documented in the debris-rich basal ice of GRIP and Dye-3 (Souchez et al., 1995a, 2006; Verbeke et al., 2002) and additional support comes from observations of high CH_4 and CO_2 concentrations in subglacial runoff (Adnew et al., 2025; Christiansen et al., 2021; Lamarche-Gagnon et al., 2019; Pain et al., 2021). Two mechanisms could explain this accumulation: (i) CH_4 and CO_2 release from buried soils and sediments, including permafrost, which may slowly outgas into the debris-rich ice (Weitemeyer and Buffett, 2006; Souchez et al., 2006; Verbeke et al., 2002), and (ii) in situ methanogenesis and respiration at the ice-bed interface (Wadham et al., 2008).

For (i), Arctic soils and sediments are characterized by abundant organic matter and often experience anoxic conditions, both of which are favourable for methanogenesis (Tarnocai et al., 2009; Wagner et al., 2005). Their organic content can vary by orders of magnitude, strongly influencing the amount of CH_4 and CO_2 that can accumulate (Serrano-silva et al., 2014; Tarnocai et al., 2009; Wagner et al., 2005; Weitemeyer and Buffett, 2006). Consequently, the initial CH_4 and CO_2 inventory beneath an

https://doi.org/10.5194/egusphere-2025-6204
Preprint. Discussion started: 13 January 2026

ice sheet is largely determined by the characteristics of the preglacial ecosystems that once occupied the area prior to the ice-sheet buildup (Stibal et al., 2012; Wadham et al., 2008). The nature of the incorporated substrate remains unknown at GRIP, but Tison et al. (1998) and Souchez et al. (2006) hypothesized the presence of a marsh or a bird breeding area, based on biomarkers as well as gas composition and isotopic data. Sediments extracted from the GISP2 debris-rich ice preserved 0.3 to 1.7% of organic carbon likely originated from a former tundra soil (Bierman et al., 2014). At Camp Century, the substrate is identified as a succession of sedimentary deposits, from a basal till to fluvial sediments (Bierman et al., 2024; Christ et al., 2024, Collins et al., 2025). These sediments materials contain carbon rich material, such as terrestrial plant macrofossils (Christ et al., 2021). As the ice sheet grows, buried substrates become increasingly insulated, causing gradual warming from retained geothermal heat (Cuffey and Paterson, 2010). This rise in temperature may progressively release CH_4 and CO_2 at the ice-bed interface, potentially enhancing both microbial activity and temperature-dependent physical or chemical processes.

For (ii), subglacial environments are commonly characterized by abundant organic matter and anoxic conditions, providing favourable conditions for methanogenesis (Boyd et al., 2010; Foght et al., 2004; Sharp et al., 1999; Skidmore et al., 2000; Wadham et al., 2008; Wagner et al., 2005). In our study, we used a DNA-based approach and did not focus on viable organisms, however viable microorganisms, including methanogens, are commonly observed in subglacial waters (Boyd et al., 2010; Lanoil et al., 2009; Sharp et al., 1999; Skidmore et al., 2000; Stibal et al., 2012) Our DNA measurements (section 4.3) show that many of the key genes involved in methanogenesis are observed at the base of the Camp Century ice core, indicating that the genetic potential for in situ CH_4 production is present (Figs. 1d).

Methanogenesis in subglacial environments depends on three conditions: anoxia, presence of water and a suitable carbon substrate (Wadham et al., 2008). Anoxic conditions (i.e., defined as O_2 concentration less than 6.25×10^{-5} mol kg^{-1}, Vaquer-Sunyer and Duarte, 2008) are reached 1.25 meters above the ice- bed interface at Camp Century and 0.5 meters from the ice-core bottom at GRIP (Fig. B5). In both ice cores, the O_2 mixing ratio and concentration decreases with the first appearance of the debris and keep decreasing with depth. Multiple processes can consume oxygen in subglacial environments, ranging from abiotic processes such as sulphide oxidation (Tranter et al., 2002; Yde et al., 2010) to biotic processes like respiration which produces CO_2 (Sharp et al., 1999; Skidmore et al., 2000; Souchez et al., 2006; Tung et al., 2006; Yde et al., 2010). The presence of water is expected within liquids veins along ice crystal boundaries and at the interfaces between ice crystal and debris, even under sub-freezing conditions (Marath and Wettlaufer, 2020; Ng, 2021; Rempel et al., 2002). As we already mentioned before, organic carbon availability depends on the nature of the buried soils and sediments but is expected in most cases to be sufficient for respiration and methanogenesis in the buried soil and sediments (Wadham et al., 2008).

Despite the fact that all these conditions are potentially encountered in the deepest layers of the debris-rich ice, our data cannot support active methanogenesis within the ice itself. DNA analysis indicates that the methanogenesis metabolic pathway is incomplete in most samples, except those collected near the ice-bed interface at Camp Century (Figs. 1d, j). Furthermore, CH_4

https://doi.org/10.5194/egusphere-2025-6204
Preprint. Discussion started: 13 January 2026

accumulation in the debris-rich ice layer occurs above the depth at which anoxic conditions are reached. Thus, CH_4 appears to originate mainly from the bed material. It is transported into the overlying ice by mechanical mixing (Sect. 4.2.1), may experience gas loss (Sect. 4.2.2), and can be partly replenished through diffusion (Sect. 4.2.3)

4.2 Gas transport in debris-rich ice

In this section, we consider the three major processes that will control gas transport within the debris-rich basal ice, i.e. mechanical mixing (4.2.1), gas loss (4.2.2) and gas diffusion (4.2.3). These three processes will act concurrently or subsequently, therefore potentially considerably complexifying the gas profiles interpretation.

4.2.1 Mechanical mixing

Shearing and folding are well-established mechanisms by which mechanical mixing entrains debris into basal ice (Alley et al., 1997; Knight, 1997), potentially incorporating sediments-rich ice with low gas content, low O_2 concentrations and high CO_2 and CH_4 concentrations. Souchez et al (1995) attributed gas variations in the GRIP basal ice to mechanical mixing between buried sediments or soils and debris-free ice. This is supported by the co-variation of ice $\delta^{18}O$, debris content, and gas composition (Fig. 4). Basal properties, illustrated in Fig 4 a,b for ice $\delta^{18}O$, CH_4, and debris content, align reasonably well with a mixing line between debris free bottom ice and a basal endmember (Souchez et al., 1995; see also Fig. B1 for all measured properties).

The consistency of this mixing pattern across independent variables, each governed by different processes, provide compelling evidence for mechanical mixing as entrapment mechanism for CH_4 and CO_2 in the GRIP basal ice section. The biogeochemical properties of the local end-member likely reflect inputs from relict soils buried beneath the ice sheet, where organic matter decomposition occurred under prevailing anoxic conditions, possibly also from local firn, which may have been partly or fully modified by inputs from the underlying soil (Souchez et al., 2006; Tison et al., 1998), or in situ CH_4 and CO_2 production in the subglacial environment (Wadham et al., 2008). However, deviations from the mixing line observed in some samples suggest that additional processes may influence the distribution of properties (Fig. 4a), such as differential diffusion rates near concentration peaks (Fig. 4b). These peaks may indicate localized injections of substrate material caused by shearing processes (Tison et al., 1994).

For Camp Century, mechanical mixing alone cannot explain the observed distribution of ice $\delta^{18}O$, debris content and gas composition. A two-component mixing model, between a “local debris-free ice endmember” and a “basal local endmember”, fails to reproduce the observations (Fig. 4a, b; Fig B2). More complex mixing models likewise fail to capture all observed features. The initial increase in the mixing ratios of N_2, Ar, CO_2, and CH_4 when debris first appears, at 16.8 m above the bed, may be attributed to either minor mixing with a basal endmember or to a net in situ O_2 consumption caused by respiration or weathering processes (Tranter et al., 2002). Net O_2 consumption would reduce the total number of moles of gas, thereby

https://doi.org/10.5194/egusphere-2025-6204
Preprint. Discussion started: 13 January 2026

proportionally increasing the mixing ratio of other gas species, as observed (Fig. 1). In any case, in the absence of refreezing processes, the incorporation and presence of debris into the basal ice must result from mechanical mixing such as shearing and folding at the sediment-ice interface (Alley et al., 1997; Hubbard et al., 2009; Knight, 1997; Souchez et al., 1995a). Nevertheless, the gas composition clearly shows that superimposed physical and biogeochemical processes affect the mechanical-mixing signal at Camp Century. The combined influence of physical and biochemical processes, including gas-loss mechanisms (4.2.2), upward diffusion (4.2.3), likely obscure the signal inherited from mechanical mixing.

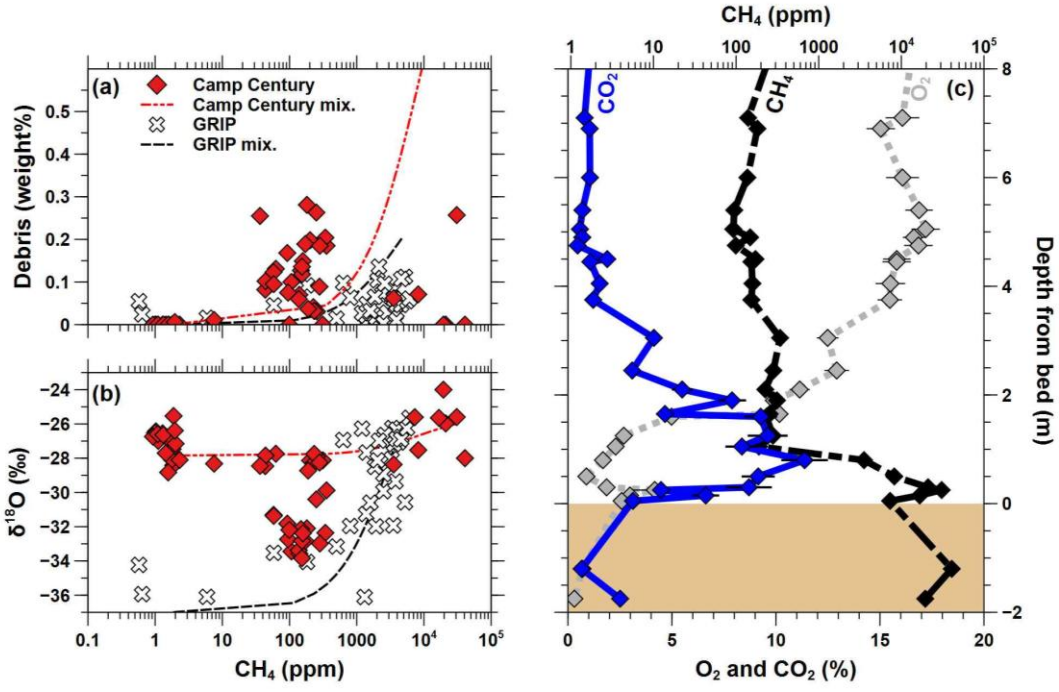

Figure 4: Ice properties ($\delta^{18}O$ of ice water, CH_4, CO_2 and debris content; a, b) in GRIP and Camp Century basal sequence. The mixing line considers a meteoric and a basal endmember specific to each ice core (Annexe B). (c) Variations of gas concentrations (CO_2, CH_4, and O_2) in the last 8 meters of Camp Century basal sequence and in the sediments. Note that CH_4 content is in log scale.

4.2.2 Gas expulsion at the ice-bed interface

At Camp Century, the gas content in the ice above the first appearance of debris is much lower (58.4 ± 2.3 ml kg^{-1}) compared to what would be expected from meteoric ice formed at the surface of the present-day ice sheet (Martinerie, 1990). Lower gas content in basal ice indicates that, in addition to the transport by mechanical mixing (sect. 4.2.1) gases were also expelled from the ice matrix while debris are incorporated during transport in the vicinity of the bed (Fig. 3a, g). Gas expulsion can occur independently of debris incorporation, like during flow obstacle of hard bedrock (Weertman, 1972). In both locations, data point toward a gas loss which can affect both the debris-free ice and the debris-rich ice layers.

https://doi.org/10.5194/egusphere-2025-6204
Preprint. Discussion started: 13 January 2026

In agreement with cold-bed conditions at both sites over time (MacGregor et al., 2016b), water isotope data and ice facies from GRIP and Camp Century rule out a freeze-on mechanism as the cause of both debris incorporation and gas depletion (Figs. 1 and 2; Souchez and Jouzel, 1984). Instead, pressure variations at the ice-bedrock interface, caused by irregular bedrock topography, may generate pressure gradients between gas inclusions and subglacial cavities. These gradients could drive gas loss as ice flows over bedrock protuberances (Knight, 1997; Weertman, 1972). The efficiency of this mechanism likely depends on the size and shape distribution of these protuberances, with smaller, more frequent protuberances (Budd, 1970), potentially enhancing gas loss near the sediment-ice interface, as observed (Fig. 3a,g).

Being located at the ice sheet margin and at lower elevation, Camp Century ice has experienced more dynamic conditions than GRIP. This is shown by changes in the ice fabrics of Camp Century, with re-orientation of the fabrics and decrease in the crystal size, in the last 300 meters of the ice core (Herron and Langway, 1982). In the debris-rich section, ice crystals exhibit a highly preferred orientation of the optic axes in the last 10 meters above the bed, indicating a zone of relatively high shear deformation (Herron et al., 1979). At GRIP, crystal size increases until the first appearance of debris (Thorsteinsson et al., 1997; Tison et al., 1994). Radar estimates of the ice-bedrock interface suggests that the basal ice sequence is thinner at GRIP, where the top 1.5 meters of the retrieved 5 meters of basal ice shows alternation of coarse crystals with weak fabrics and fine crystals with single maximum fabrics (Tison et al., 1994), suggesting local discrete shearing and a less vertically extensive dynamic flow history compared to Camp Century.

An additional mechanism potentially contributing to both gas loss and the formation of dispersed facies is the downward migration of particles in a positive temperature gradient via thermal regelation (Marath and Wettlaufer, 2020). When particles are embedded in ice, thin liquid films form around them due to local melting. In the presence of a basal temperature gradient, particles migrate downward through repeated melting and refreezing, with the rate depending on particle size (Marath and Wettlaufer, 2020). If debris is initially injected by shearing, size-dependent regelation can spread particles vertically at different rates, forming a dispersed facies. This process may also enhance gas loss if particles and their surrounding liquid films reach the sediment–ice interface. Additional factors, such as enlargement of the inter-crystalline liquid layer or localized pressure variations downstream of bedrock obstacles, could further promote particle migration and gas expulsion (Rempel, 2005; Rempel et al., 2002)

To assess whether gas loss is accompanied by fractionation among gas species, Figure 5 compares the measurements to an idealized scenario where gas loss is the only process affecting the basal section of Camp Century, assuming no fractionation between gas species (Appendix B). Starting from the sample with the highest gas content, 17.65 meters above the bed, the O_2 concentration follows the expected gas loss trend until the first appearance of debris, beyond which the O_2 concentration deviates from the idealized gas loss trend, due to consumption by chemical weathering or respiration (Fig. 5a).

https://doi.org/10.5194/egusphere-2025-6204
Preprint. Discussion started: 13 January 2026

Ar concentrations also follow the idealized gas loss trend in debris-free ice but show a deviation in debris-rich ice, with accumulation near the sediment-ice interface (Fig. 5b, c). This accumulation is possibly due to radiogenic Ar production and diffusion from the bed, as discussed in the following section. N_2 does not appear to differ markedly from the idealized gas loss trend, although the samples exhibiting the strongest deviations in Ar also show a slight departure from the idealized gas loss trend. However, because N_2 is the most abundant gas, contributions from diffusion from the bedrock or biological production are more difficult to detect in bulk concentrations (mol N_2 kg^{-1}), even though they are more apparent in the mixing ratio (Fig. 3).

Overall, observations from the debris free bottom ice, including mixing ratios close to atmospheric values for major gas species (N_2, O_2, Ar; Fig. 3c, e, f), suggest that gas loss occurs without fractionation, affecting all gas species equally and aligning with the mechanisms described above (Fig. 5a, b, c). This is further supported at GRIP; measurements are not statistically different that the idealized gas loss trends, except for O_2 (loss) and CH_4 (accumulation), because of the biological activity (Annexe B, Fig. B3).

In both GRIP and Camp Century ice, CH_4 concentrations deviate from the expected gas loss trend, with the highest values observed in the deepest ice layers (Figs. 5d and B3d). A similar behaviour is observed for CO_2 (Fig. B4), suggesting that CH_4 and CO_2 are either preferentially preserved or actively produced. While mechanical mixing and gas expulsion affects gas behaviour near the ice-bed interface, the accumulation of Ar and potentially N_2 points to a contribution from diffusion.

https://doi.org/10.5194/egusphere-2025-6204
Preprint. Discussion started: 13 January 2026

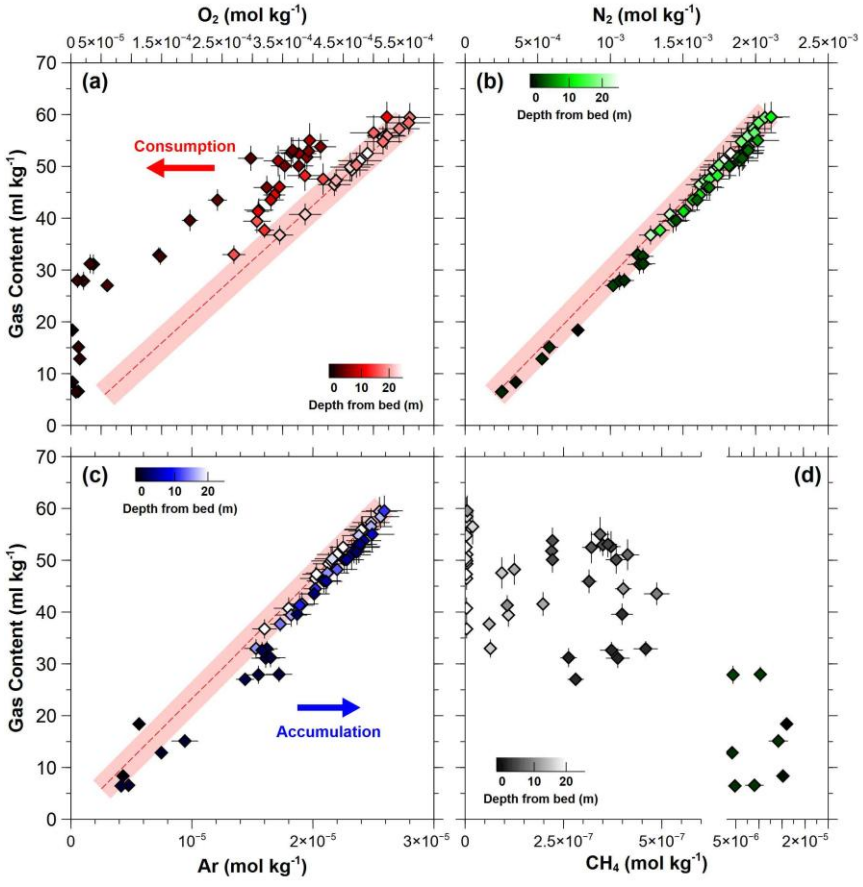

Figure 5: Variations in the concentrations of (a) O_2, (b) N_2, (c) Ar, and (d) CH_4 (mol kg^{-1}) in Camp Century debris-rich ice as a function of gas content (ml kg^{-1}). The colour gradients represent the depth of measurement, with lighter points indicating debris-free ice above the debris-rich section. The red curve and associated error bars (red envelop, 1 standard deviation) represent the ideal scenario where gas loss occurs without fractionation between gas species (Appendix B).

4.2.3 Gas diffusion

N_2 and Ar is particularly useful for constraining diffusion processes near the sediment-ice interface due to its well-understood production mechanisms and their largely its inert behaviour once diffusing into the ice.

At Camp Century, N_2 profile shows a non-steady state pattern of diffusion defined by boundary conditions with relatively enriched basal endmember (mixing ratio higher than 93%) and a progressive enrichment from present-day atmospheric composition to 87 - 88 % at the ice-sediment interface (Fig. 3f). We have two main hypotheses to explain the high mixing ratio in the sediment. First, denitrification under anoxic conditions, such as those found in the sediments (Boyd et al., 2010; Foght et al., 2004), can lead to N_2 accumulation. This is supported by the presence of denitrification genes across the sequences

https://doi.org/10.5194/egusphere-2025-6204
Preprint. Discussion started: 13 January 2026

(Table A2). Second, the selective removal of more soluble gas species by percolating water in the sediments (i.e., leaching processes), can lead to relative N_2 enrichment, due to its lower solubility compared to O_2, Ar, and CO_2 (Weiss et al., 1972).

In solid ice where gas inclusions are not interconnected (as is likely the case here), molecular diffusion occurs through the ice lattice via gas molecules dissolved in the solid phase, which are in equilibrium with air bubbles or clathrates (Ahn et al., 2008; Ikeda-Fukazawa et al., 2005; Oyabu et al., 2021). This process involves two steps: (a) gas transfer from the gas inclusion to the surrounding ice, where concentration depends on the mixing ratio in gas inclusions according to Henry's law; (b) diffusion within the solid ice downside a concentration gradient. Dissolved gas concentrations are higher near gas inclusions with higher mixing ratios, even if the total gas content is lower. Consequently, N_2 diffuses upward from the sediments into the basal ice along a gradient in the mixing ratio (Fig. 3f).

Radiogenic Ar is produced in the Earth's crust through radioactive decay of ^{40}K with has a half-time life of 1.25×10^9 yrs (Bender et al., 2010) and thus, is expected to accumulate in the bed material beneath the ice. The non-steady state pattern of diffusion is not observed at GRIP ice core where the drilling did not reach the bed, but it is clear at Camp Century where Ar is progressively enriched from 0.95 ± 0.05 % in the debris-free ice to 1.57 ± 0.05 % at the ice-sediment interface. However, the accumulation is surprisingly heterogenous in the bed material (Unit 2) with 2 measured Ar mixing ratios of 1.12 ± 0.06 % and 0.67 ± 0.04 %.

The origin of the ice-rich layers in the sediments (Unit 2), where gas composition was measured, remains unclear at this time (basal ice remnant-local or dynamically advected from inland or local firn). Unit 2 lies beneath fluvial deposits (Units 3, 4, and 5) that are in contact with the bed–ice interface and may therefore contain a distinct gas composition (Bierman et al., 2024; Collins et al., 2024). In addition, selective removal of more soluble gas species by percolating water in the sediments/firn (i.e., leaching) can enrich N_2 owing to its lower solubility relative to O_2, Ar, and CO_2 (Weiss et al., 1972). It is therefore plausible that Unit 2 experienced significant leaching, resulting in both substantial gas depletion (gas content < 25 ml kg^{-1}) and a local depletion of Ar.

The presence of fluvially transported material deposit (Bierman et al., 2024; Collins et al., 2024) could indeed indicate deposition under warmer conditions above the freezing point of water. An alternative hypothesis is that the Ar diffusion profile observed in ice above the ice-bed interface was inherited from an upstream locality, and subsequently advected to its present position by ice flow. Such a scenario would imply a decoupling between the debris rich, Ar-rich ice and the underlying, Ar-pool bed material. Thus, the Ar we measured in bed material (Units 2) do not represent the local endmember, potentially explaining the heterogeneity in Ar mixing ratio at the ice-bed interface.

https://doi.org/10.5194/egusphere-2025-6204
Preprint. Discussion started: 13 January 2026

Reproducing the observed non-steady state diffusion profile of N_2 and Ar requires a permeation coefficient (i.e., the product of solubility and diffusion coefficients) several orders of magnitude higher than values reported in literature for molecular diffusion through the ice lattice (Oyabu et al., 2021, and references therein). This discrepancy may be resolved by the presence of a network of intergranular water veins that "short-circuits" the slow diffusion within ice lattices (Ng, 2021; Rempel, 2005). These veins allow higher effective diffusion coefficients, which, over the expected age of the ice (< 416 ± 38 ka; Christ et al., 2023), would be sufficient to produce the observed non-steady state diffusion profile of N_2 and Ar near the sediment-ice interface (Fig. 1).

4.3 Subglacial methane preservation in debris-rich ice

4.3.1 Methane preservation and consumption in the ice

Gas profiles and microbial DNA sequencing indicates a greater potential for in-situ CH_4 consumption at Camp Century compared to GRIP (Fig. 3d, j; Appendix A).

The CH_4 profile at Camp Century aligns with a non-steady state pattern of diffusion in which CH_4 is produced by methanogenesis in the sediments and transported by diffusion into the basal ice (Figs. 1d and 4c). The transport of CH_4 by diffusion is expected to occur more rapidly than that of Ar due to its smaller molecular size, thus resulting in CH_4 concentrations decreasing more slowly away from the sediment interface compared to Ar. This is the opposite to what we observe in our samples since CH_4 concentrations decrease more sharply closer to the sediment interface than Ar (i.e., 1.0 vs. 2.0 meters, respectively, Fig. 1d, e). This observation suggests that CH_4 may be consumed during its upward transport through the ice.

The potential consumption of CH_4 by biological CH_4 oxidation is further supported by the profiles of O_2, CH_4 and CO_2 (Fig. 4c). In oxic environments, methanotrophs utilize molecular oxygen to oxidize CH_4 to CO_2, incorporating a fraction of carbon into biomass during the process (Hanson and Hanson, 1996). In anoxic environments, anaerobic methanotrophs utilize alternative electron acceptors, such as sulfate and nitrate, to oxidize CH_4 (Serrano-silva et al., 2014). Assuming diffusion-dominated transport, the gradients of CH_4 and O_2 (or other electron acceptors) define the zone where CH_4 oxidation occurs, leading to the formation of a CO_2 peak (i.e., the reaction product) at the region where CH_4 is being oxidized (Urmann et al., 2007). In our profiles, a sharp decline in CH_4 concentration coinciding with a CO_2 peak near the sediment–ice interface strongly supports in situ CH_4 oxidation by methanotrophy (Fig. 4c).

To assess whether the observed decrease in CH_4 can quantitatively account for the CO_2 peak, we estimate that 1.6×10^{-5} mol kg^{-1} of CH_4 is consumed between the ice-bed interface and 4.0 meters above it. Over the interval from 0.8 to 4.0 meters above the interface, 9.8×10^{-5} mol kg^{-1} of CO_2 is accumulated. This suggests that at least 20% of the observed CO_2 accumulation could result from methanotrophy. Since CH_4 is continuously produced in the sediment and diffuses upward into the ice and

https://doi.org/10.5194/egusphere-2025-6204
Preprint. Discussion started: 13 January 2026

given that some CO_2 dissociates into carbonate and bicarbonate ions in the presence of water (Tranter et al., 1996, 2002), this is likely a conservative estimate. Nevertheless, it indicates that the changes in CH_4 and CO_2 concentrations are of the same order of magnitude, supporting our hypothesis.

Near the ice-bed interface at Camp Century, DNA analyses reveal the presence of the complete metabolic pathway for anaerobic methane oxidation (AOM), along with genes associated with consortia of anaerobic methanotrophic archaea and sulfate reducing bacteria. These findings support our interpretation that methanotrophy can consume CH_4 as it diffuses upward at the sediment–ice interface (Fig. 3d; Table A1). In contrast, evidence for aerobic methane oxidation is limited. Microbial DNA sequencing indicates only partial representation of the aerobic pathway, with a completeness of 75 % near the ice-bed interface.

Vertical gas profiles at GRIP and their synchronicity with other ice properties such as $\delta^{18}O$ and debris content suggest that CH_4 is predominantly entrapped in the basal ice through mechanical mixing. As the ice core at GRIP did not reach the bedrock, it is possible that the methanotrophic activity, along with the non-steady diffusion profile for CH_4 observed at Camp Century near the ice-bed interface, was not captured. While this interpretation is consistent with the relatively similar N_2 and Ar concentrations in the basal ice at GRIP and the section spanning 3 to 17 m above the ice-bed interface at Camp Century, the profiles for O_2, CO_2 and CH_4 differ markedly between the two sites (Fig. 3).

CH_4 mixing ratios remain elevated at GRIP even in the presence of O_2 (above 5 % O_2 mixing ratio), suggesting lower methanotrophic activity compared to Camp Century. Metagenomic data support this interpretation, showing that methanotrophy-related genes are rare in the GRIP basal ice (< 6 % pathway completeness; Figs. 3d, j; Table A1), although this result is based on only two samples. Additionally, although methanotrophy preferentially oxidizes ^{12}C-bearing CH_4 molecules with a large isotope effect (Coleman et al., 1981; Kinnaman et al., 2007), no inverse relationship is observed between CH_4 concentration and CH_4 vs $\delta^{13}C$ at GRIP (Souchez et al., 2006), providing further evidence against active methanotrophy at this site.

4.3.2 Controls on subglacial methanotrophy

Both Camp Century and GRIP currently experience cold bed conditions (i.e., -13°C and -9.2°C, respectively; McGregor et al., 2016) and exhibit similar facies and debris content (Fig. 1). Supporting evidence that methanotrophic activity appears to be absent or minimal at GRIP includes the occurrence of elevated CH_4 mixing ratios under oxic conditions, the near absence of methanotrophy-related genes, and the lack of an inverse correlation between CH_4 concentration and CH_4 $\delta^{13}C$.

Warmer basal conditions at Camp Century may have occurred during glacial maxima ice ages, or during transient periods such as glacial inceptions, associated with an “transient” increase in local ice thickness of approximately 600 m relative to present-

https://doi.org/10.5194/egusphere-2025-6204
Preprint. Discussion started: 13 January 2026

day values (Lauritzen et al., 2025; Simpson et al., 2009). Increased ice thickness during ice ages, would reduce the efficiency of heat removal at the bed through conduction, allowing geothermal heat to accumulate in the subglacial environments (Cuffey and Paterson, 2010). This would promote metabolic activity. In contrast, the more stable conditions at GRIP, characterized by less variability in ice thickness over time, vertical velocity, and surface temperature, have maintained consistently cold bed conditions throughout both glacial and interglacial periods (MacGregor et al., 2016a).

Another factor influencing methanotrophic activity is the quality of the organic matter incorporated within the debris-rich ice might differ between locations (Wadham et al., 2008). Even if similar vegetation was initially buried at both GRIP and Camp Century, the present-day gas content reflects prolonged sediment-ice interaction, over ~ < 400,000 yrs at Camp Century versus ~1 million years at GRIP (Christ et al., 2021; Willerslev et al., 2007). Over time, the transformation of labile organic matter into a more recalcitrant pool suggests that the much older basal ice at GRIP likely contains less bioavailable carbon, potentially limiting microbial processes such as methanotrophy.

Overall, the primary control on the preservation of a methanotrophy signature is likely the thermal state at the base of the ice sheet. Accordingly, O_2 and CH_4 profiles across the bed material-ice interface are expected to differ markedly between warm- and cold-bed settings (Fig. 6). Under warm-bed conditions, atmospheric gas concentrations in the overlying ice would persist down to the bed, releasing O_2 in the subglacial water and sediments, while CH_4 would increase downward into the sediments, coupled with a corresponding decrease in O_2. Such a distribution has been reported in subglacial Lake Whillans beneath the West Antarctic Ice Sheet (Michaud et al., 2017). This is further supported by measurements at NGRIP, drilled above a warm bed with a melting flux at the base, where CH_4 concentrations and $\delta^{18}O$ of O_2 values remain within the atmospheric range in the last meters of the core (Capron et al., 2010; Landais et al., 2006). In contrast, under cold-bed conditions, CH_4 and O_2 gradients would extend upward into the ice, as observed at GRIP and Camp Century, and the CH_4 being produced in the subglacial environment will remain preserved to some extent in the ice depending on the potential for in situ methanotrophy. Additional measurements in a basal ice section in a warm-bed condition would be particularly valuable for distinguishing between these two behaviours.

https://doi.org/10.5194/egusphere-2025-6204
Preprint. Discussion started: 13 January 2026

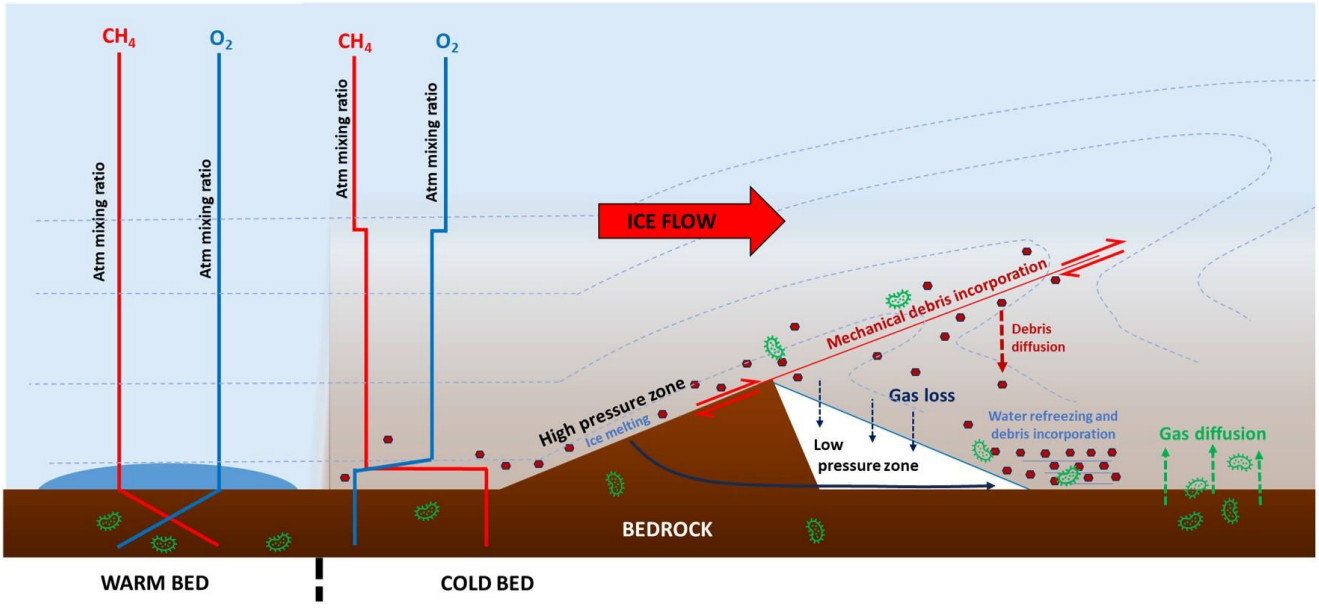

Figure 6: Schematic view of CH_4 sources and sink under ice sheet (not to scale). CH_4 accumulates in subglacial environments either from the release of gases from buried soils and sediments beneath the ice sheet or via in situ methanogenesis. Under warm basal conditions, CH_4 produced in the bedrock is removed via subglacial runoff at the ice/bedrock interface. Meanwhile, the release of O_2 from the basal melting of debris-free ice, characterized by a near-atmospheric gas composition (atm mixing ratio), can potentially support CH_4 consumption either in the subglacial runoff or in the underlying sediments. In cold-based conditions, gas loss and water refreezing are influenced by pressure variations induced by ice flow over bedrock protuberances. Debris can be incorporated into the ice either through mechanical mixing or by in-situ water refreezing. CH_4 produced in the bed material is trapped in the debris-rich ice through mixing and diffusion. Depending on the conditions, methanotrophy in debris-rich ice may acts as a sink, consuming part of the CH_4 accumulation.

5 Conclusion

Our study reveals both marked differences and similarities in the production, transport, and consumption of greenhouse gases in the basal ice sections from Camp Century and GRIP, located at the northwestern margin and the summit of the Greenland Ice Sheet, respectively. In both basal ice sections, we observe substantial accumulations of CO_2 and CH_4, accompanied by O_2 consumption. These accumulations likely result either from the release of gases from buried soils and sediments beneath the ice sheet or from in situ respiration and methanogenesis within the subglacial environment. The latter is supported by methanogenic analyses that confirm the potential for CH_4 production and consumption near the bed–ice interface at Camp Century.

https://doi.org/10.5194/egusphere-2025-6204
Preprint. Discussion started: 13 January 2026

The transport of CO_2 and CH_4 into debris rich ice occurs via distinct mechanisms (Fig. 6): at GRIP, it is primarily driven by mechanical mixing through shearing and folding from at least 7 meters above the bedrock, whereas at Camp Century, diffusion across the bed–ice interface dominates in the bottom 6 meters. Superimposed on these transport processes, partial gas loss also occurs, either due to pressure gradients at the bed–ice interface, caused by irregular bedrock topography, or through downward debris and gas migration by thermal regelation.

Once CH_4 is trapped in the debris-rich ice, it may be oxidized via methanotrophy if conditions are favorable. At Camp Century, such conditions appear to exist, as evidenced by (i) vertical profiles of CO_2 and CH_4, showing a CO_2 peak where CH_4 is oxidized during its upward diffusion into the ice, and (ii) metagenomic data revealing a complete methanotrophy pathway near the ice-bed interface. In contrast, at GRIP, CH_4 concentrations remain well above atmospheric levels, even more than 7 m above the bedrock, despite the presence of O_2, and the methanotrophy pathway is poorly represented, suggesting that conditions there are unfavourable for methane oxidation. This contrast may stem from either the more dynamic thermal regime at the ice-sheet margin near Camp Century, linked to glacial–interglacial difference in ice thickness leading to warmer conditions near the bed during ice ages, or the presence of older, more recalcitrant organic matter at GRIP, which may be less favourable to biological activity in the ice. Additional studies, including extended measurements in GRIP basal ice, CH_4 isotope measurements, multi-omic approaches and targeted microbiological assessments, are needed to further elucidate the metabolic potential and activity of microbial communities in contrasted subglacial environments.

Appendix A: Extended microbial DNA results in the basal ice of both Camp Century and GRIP

At Camp Century, genes encoding key enzymes for acetoclastic and hydrogenotrophic methanogenesis were detected in most of the samples with variable degrees of completeness (Fig. 3d, f, Table A1). Camp Century samples from below 6.0 meters above the sediment-ice interface also contained genes associated with methylotrophic methanogenesis. The only sample exhibiting complete gene sets for all three methanogenic pathway – acetoclastic, hydrogenotrophic, and methylotrophic – was collected at 0.25 meters above the sediment-ice interface (i.e., the deepest sample analyzed for microbial DNA). Overall, methanogenesis pathway completeness at Camp Century increased with depth (r^2 = 0.52; p-value < 0.01). At GRIP, methanogenesis pathway completeness never exceeded 50 %, with an absence of genes for acetoclastic methanogenesis (Fig. 1l, Table A1). At Camp Century, genes related to know methanogens were detected in most samples (Fig. 3f; Table A1). For GRIP, genes related to know methanogens were only detected in one of the two analysed samples.

DNA sequenced from the samples matched some — but not all — of the genes involved in methylotrophy, which refers to the metabolic ability to grow by utilizing compounds that contain no carbon–carbon bonds (Anthony, 2004). Genes associated with aerobic methylotrophy, which specifically involves organisms that use CH_4 as their sole carbon and energy source, were

https://doi.org/10.5194/egusphere-2025-6204
Preprint. Discussion started: 13 January 2026

detected in only six samples, all originating from Camp Century (Fig 3d; Table A1). Among these, the highest number of gene hits within the methylotrophy pathway was found in samples collected 0.25 meters above the sediment-ice interface (i.e., the deepest sample analyzed for microbial DNA). However, even in this sample, pathway completeness did not exceed 75%.

The hallmark genes for aerobic methane oxidation – methane monooxygenase (pmoA) and methanol dehydrogenase (MDH) (Anthony, 2004; Hakemian and Rosenzweig, 2007; Trotsenko and Murrell, 2008; Williams et al., 2005) were not detected in any of the data sets. However, genes encoding methane/ammonia monooxygenase subunit A (pmoA-amoA) were found in both the ice and the inclusion of the deepest samples analyzed at Camp Century. This gene encodes a sequence-divergent particulate monooxygenase (pXMO) that is critical in the first steps of methane oxidation in the *Methylomonas*, *Methylobacter* and *Methylomicrobium* genera (Tavormina et al., 2011). Genes encoding enzymes in the ribulose monophosphate (RuMP) pathway (K08093 and K08094), one of the key pathways used by methylotrophs to assimilate formaldehyde (Chistoserdova, 2011), were only detected in the deepest samples analyzed at Camp Century, where partially complete methane oxidation pathways were observed. An exception was one GRIP sample collected 1.08 meters from the bottom, which also contained RuMP marker genes.

A total of five methylotrophic genera were detected in some samples (Fig. A1; Table A1). The dominance of *Methyloceanibacter*, a pmoA-negative methylotroph specialized in anaerobic methanol and DMS oxidation, is consistent with our functional data and could explain the detection of aerobic methylation genes despite incomplete pathways. Its co-occurrence with sulfate-reducing bacteria (SRB) suggests syntrophic methanol-to-sulfate coupling. Other methylotrophs show niche specialization: *Methylibium* mediates sulfate-dependent methanol oxidation, while *Methylorubrum* scavenges methanol in methanogen-rich zones. Altogether, this supports the presence of a pmoA-independent methylotrophic community primarily processing methanol and DMS, rather than methane.

Anaerobic oxidation of methane (AOM) occurs via three known pathways: (i) sulfate-dependent (S-DAMO), where anaerobic methanotrophic archaea (ANME) oxidize methane via reverse methanogenesis, supporting sulfate-reducing bacteria (SRB) in sediments (Boetius et al., 2000; Krüger et al., 2003); (ii) nitrate/nitrite-dependent (N-DAMO), mediated by NC10 bacteria and ANME archaea, coupling methane oxidation to denitrification (Ettwig et al., 2010); (iii) and metal-dependent (M-DAMO), which uses Mn^{4+}/Fe^{3+} as electron acceptors (Egger et al., 2015), although its exact mechanism remain unclear.

Genes encoding key enzymes involved in AOM were detected in most samples, although not all the genes implicated in the pathway were detected in each case (Fig. 3d, j; Table A1). The Camp Century samples at 0.25 meters (i.e., the deepest sample analyzed for microbial DNA) and at 6.0 meters above the sediment-ice interface showed again the highest pathway completeness (100% and 45%, respectively). These included complete hdrABC complexes (K03388-K03390), the forward-acting fwdABCD complex (K00200-K00203), and cdhC (K00196), which were found exclusively in these two samples.

https://doi.org/10.5194/egusphere-2025-6204
Preprint. Discussion started: 13 January 2026

Genes related to both ANME archaea and nitrite-dependent AOM bacteria were detected in some samples (Fig A1; Table A1). Because AOM is biochemically similar to like methanogenesis, there is a risk of misannotation in metagenomic studies. To address this, we specifically searched for genes unique to AOM, as well as co-occurrence of ANME and SRB taxa in the same samples. Taxonomic markers for AOM-SRB consortia were identified in some samples, but only the deepest Camp Century sample at 0.25m above the sediment-ice interface exhibited an ANME/SRB ratio > 1, consistent with ANME-dominated syntrophy (Boetius et al., 2000). Interestingly, N-DAMO markers were also present in several Camp Century samples. The deep Camp Century sample again stood out, showing 100% AOM completion and a high ANME/SRB ratio (1.6), suggesting niche partitioning between methanotrophs. By contrast, GRIP samples collected above 4.65 meters from the bottom (bag #5499) lacked AOM genes altogether but contained N-DAMO markers, which may reflect partial pathway recruitment or low biomass, leading to incomplete detection. Taken together, the Camp Century sample at 0.25 m above the bed–ice interface, with 100% pathway completeness and an ANME/SRB ratio of 1.6, represents the strongest candidate for AOM activity. However, functional validation is required to confirm whether the detected genes translate into active methane oxidation.

Based on the metagenomic analysis, the deepest sample from Camp Century (0.25 meters above the sediment-ice interface) represents the most compelling candidate for microbial methane cycling, as it contained complete gene sets for all three methanogenic pathways and a 100% complete pathway for the anaerobic oxidation of methane (AOM), supported by a high ANME/SRB ratio of 1.6. In contrast, methanogenesis pathways at the GRIP site were always less than 50% complete. The functional data suggest the presence of a distinct methylotrophic community primarily processing methanol and DMS, rather than methane, as key genes for canonical aerobic methane oxidation were absent. Overall, the genetic potential for both methane production and consumption increased with depth at Camp Century, though functional validation is required to confirm active methane cycling.

https://doi.org/10.5194/egusphere-2025-6204
Preprint. Discussion started: 13 January 2026

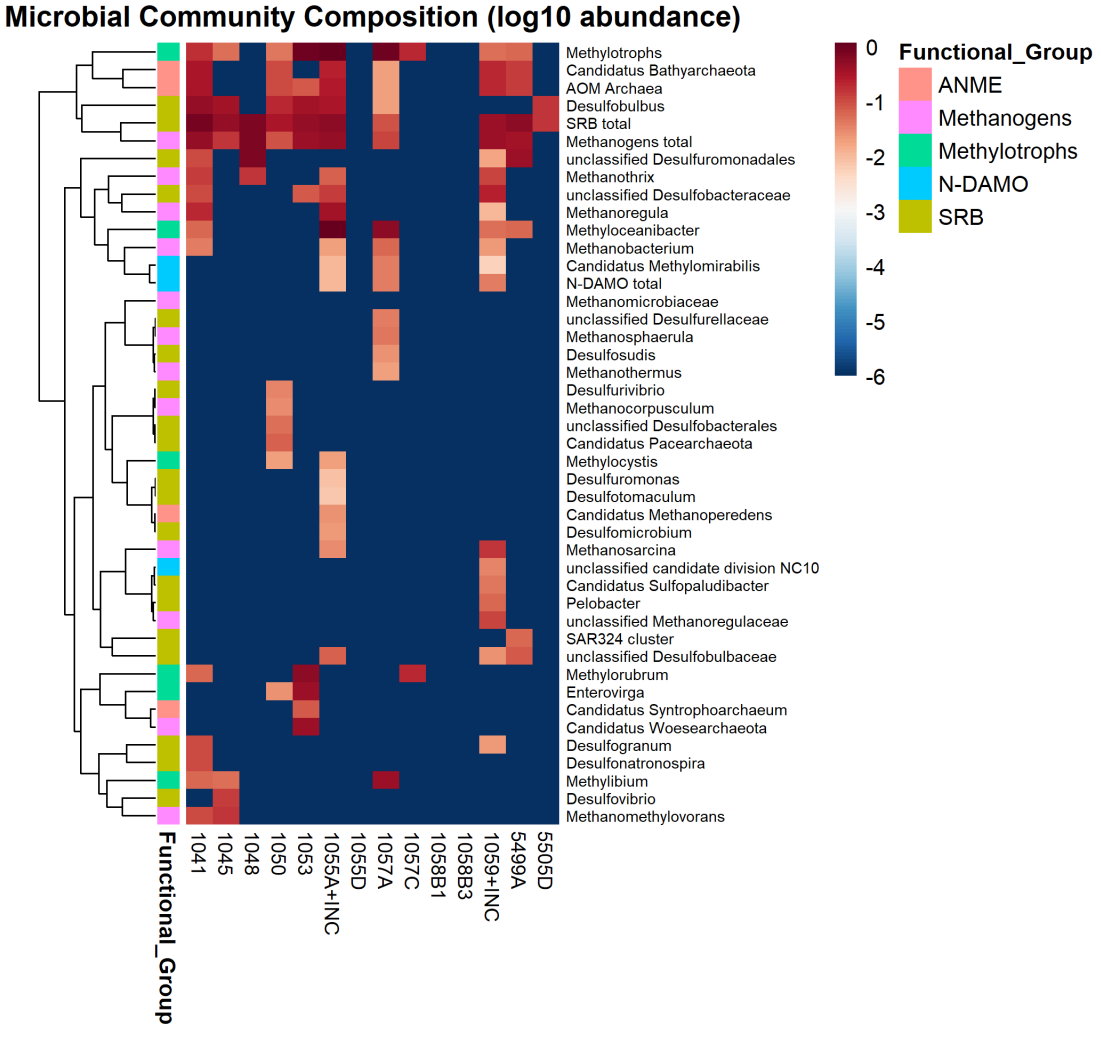

Figure A1: Heatmap of the relative abundance of the genera that constitute the microbial methane cycling community composition based sequenced metagenomes. Samples are indicated on the X-axis, while colors on the Y axis represent different functional groups of organisms.

https://doi.org/10.5194/egusphere-2025-6204
Preprint. Discussion started: 13 January 2026

Ice Core	Depth from the bottom (meters)	Methylotrophs	ANME[1]	N-DAMO[2]	Sulfate Reducing Bacteria (SRB)	Methanogens	ANME/SRB	Anaerobic oxidationof methane (AOM)	Aerobic methane oxidation	Hydrogenic Methanogenesis	Acetoclastic Methanogenesis	Methylotrophic Methanogenesis	Total Methanogenesis
Camp Century	25.80	+	+	-	+	+	0.4	18%	0%	0%	25%	0%	8%
Camp Century	19.90	+	-	-	+	+	0.0	27%	0%	13%	25%	0%	13%
Camp Century	15.60	-	-	-	+	+	0.0	0%	0%	0%	0%	0%	0%
Camp Century	12.40	+	+	-	+	+	0.4	18%	25%	0%	0%	0%	0%
Camp Century	7.10	+	+	-	+	+	0.2	18%	0%	0%	0%	0%	0%
Camp Century	6.00[3]	+	+	+	+	+	0.5	45%	50%	75%	75%	50%	67%
Camp Century	4.90	-	-	-	-	+	0.0	18%	0%	25%	25%	0%	17%
Camp Century	3.05	+	+	+	+	+	0.5	36%	25%	63%	50%	50%	54%
Camp Century	1.90	+	-	-	-	-	0.0	27%	0%	75%	50%	50%	58%
Camp Century	0.80	-	-	-	-	-	0.0	18%	25%	63%	75%	50%	63%
Camp Century	0.30	-	-	-	-	-	0.0	18%	0%	75%	50%	50%	58%
Camp Century	0.25[3]	+	+	+	+	+	1.6	100%	75%	100%	100%	100%	100%
GRIP	4.65	+	+	+	+	+	0.3	0%	0%	0%	0%	50%	17%
GRIP	1.08	-	+	-	+	-	0.0	9%	0%	13%	0%	50%	21%

[1]Anaerobic Methanotrophic Archaea

[2]Nitrate/Nitrite-dependent AOM bacteria

[3]DNA sequencing on both bulk ice samples and picked inclusions

Table A1: Table summarizing the presence and absence of key anaerobic methane oxidation taxa, in addition to the ratio of ANME and SRB, as well as pathway completeness in percent. Pathway completeness was derived by calculating the presence/absence of essential genes for each given pathway based KEGG maps.

https://doi.org/10.5194/egusphere-2025-6204
Preprint. Discussion started: 13 January 2026

Sample	Nitrogen Fixation	Nitrification (Ammonia Oxidation)	Nitrification (Nitrite Oxidation)	Denitrification	Assimilatory Nitrate Reduction	Dissimilatory Nitrate Reduction	Anammox
CC 1041	0%	0%	0%	50%	0%	66.70%	0%
CC 1045	0%	0%	0%	75%	0%	66.70%	0%
CC 1048	0%	0%	0%	25%	0%	33.30%	0%
CC 1050	0%	0%	50%	100%	50%	66.70%	0%
CC 1053	0%	0%	0%	50%	0%	33.30%	0%
CC 1055 A	0%	0%	50%	100%	50%	100%	0%
CC INC 9	33%	0%	100%	50%	100%	100%	0%
CC 1055 D	0%	0%	0%	0%	0%	0%	0%
CC 1057 A	0%	0%	50%	75%	100%	66.70%	0%
CC 1057 C	0%	0%	50%	75%	50%	66.70%	0%
CC 1058 B1	0%	0%	100%	75%	50%	33.30%	0%
CC 1058 B3	0%	0%	50%	75%	50%	66.70%	0%
CC 1059	50%	50%	100%	75%	100%	100%	0%
CC INC 12	75%	50%	100%	75%	100%	100%	0%
GRIP 5499	0%	0%	0%	0%	0%	0%	0%
GRIP 5505	0%	0%	0%	50%	0%	0%	0%

Table A2: Biological pathway completion for nitrogen metabolism for both Camp Century (CC) and GRIP samples. Samples including the identifier INC are the inclusions on which the DNA was sequenced separately from the ice. Pathway completeness was derived by calculating the presence/absence of essential genes for each given pathway based KEGG maps.

https://doi.org/10.5194/egusphere-2025-6204
Preprint. Discussion started: 13 January 2026

Appendix B: Extended gas composition results in the basal ice of both Camp Century and GRIP

The basal endmember for GRIP (Fig. B1) is the composition of the deepest sample measured at ULB, at 0.76m from the bottom of the core. The basal endmember for Camp Century (Fig. B2) is the average composition of the 2 samples measured in the sediment.

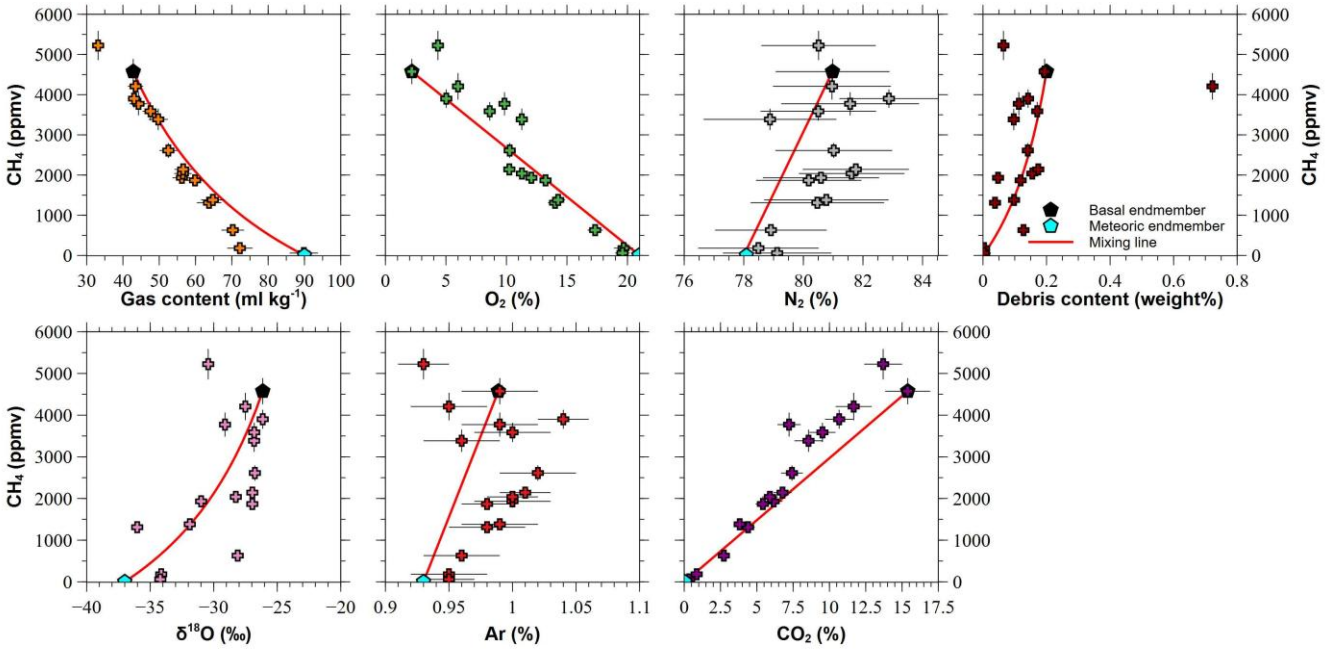

Figure B1: Relationship between CH_4 content (y-axis) and other proxies in GRIP basal ice. Red curves are the mixing line between the meteoric ice endmember (in cyan) and the basal end member (in black).

https://doi.org/10.5194/egusphere-2025-6204
Preprint. Discussion started: 13 January 2026

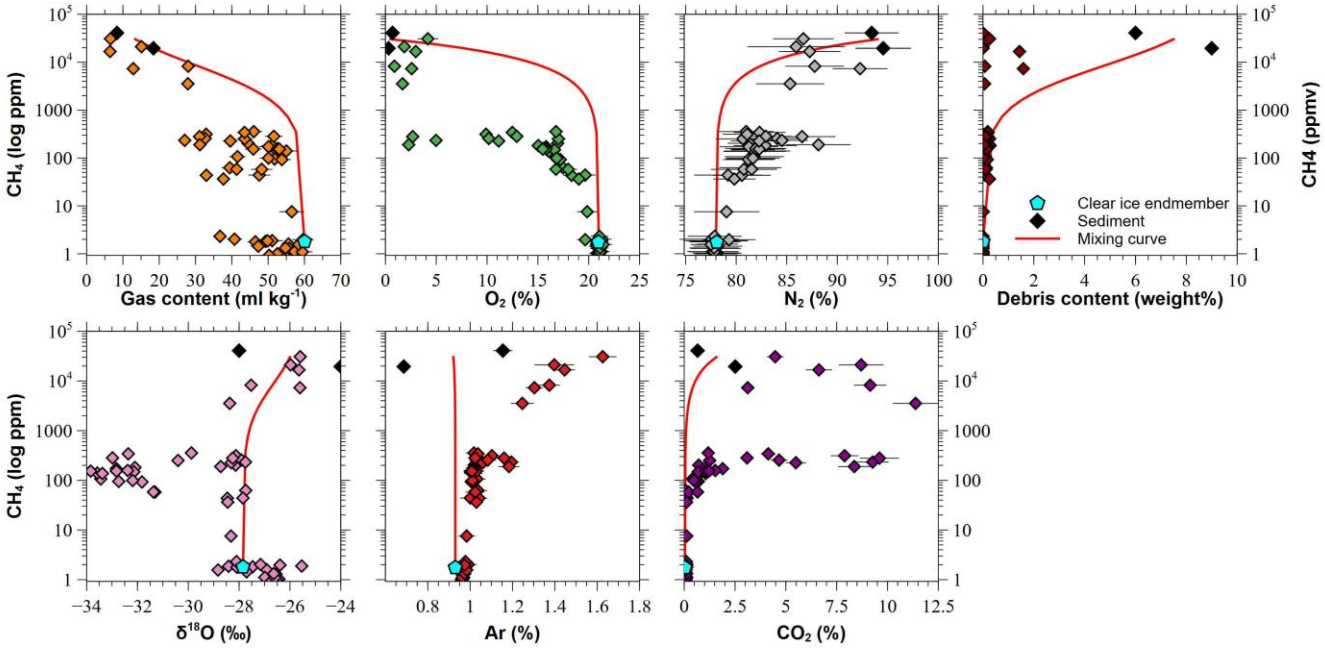

805 **Figure B2: Relationship between CH_4 (y-axis) and other proxies in the Camp Century basal sequence. The black symbols represent the two measurements taken from the sediments beneath the ice sheet. The basal endmembers are the average of the 2 sediment measurements (in black). Debris content of the sediments is from Bierman et al. (2024). The clear ice endmember (in cyan) is the average of the clear ice measurements.**

https://doi.org/10.5194/egusphere-2025-6204
Preprint. Discussion started: 13 January 2026

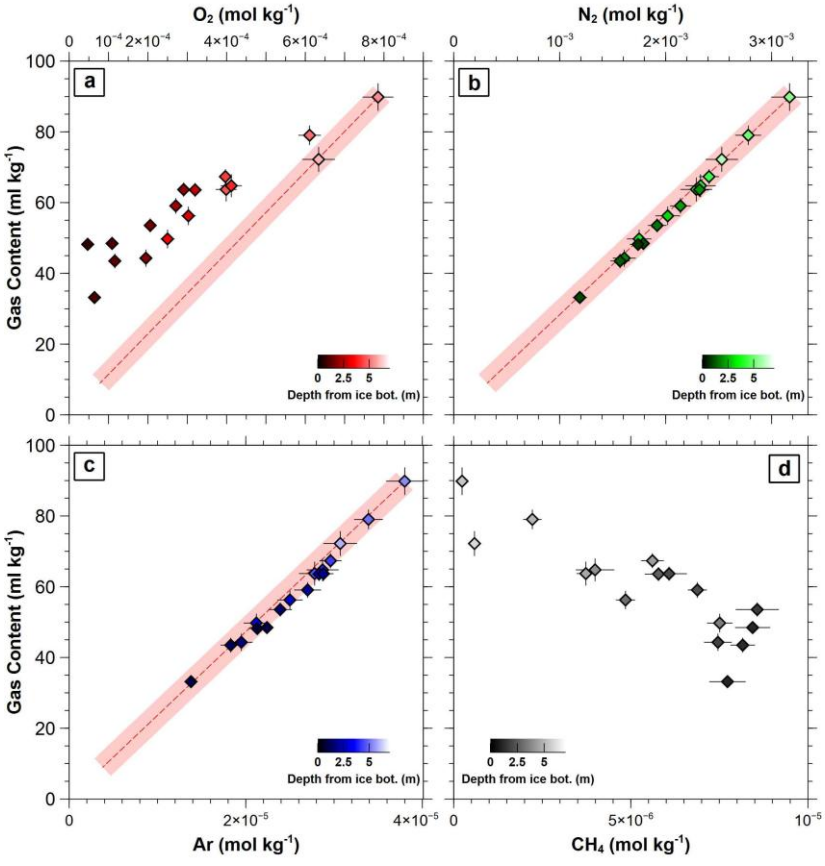

Figure B3: Variations in the concentrations of (a) O_2, (b) N_2, (c) Ar, and (d) CH_4 (mol kg^{-1}) in GRIP debris-rich ice as a function of gas content (ml kg^{-1}). The colour gradients represent the depth of measurement, with the lighter points being higher relative to the bottom of the core. The red curve and associated error bars represent the ideal scenario where gas loss occurs without fractionation between gas species.

Calculation of the ideal case of gas lost

For both Camp Century and GRIP, the starting point of the gas lost trend is the ice sample with the highest gas content. The sample is debris-free for Camp Century and debris-rich for GRIP (Table B1). From this starting point, the gas content (GC) is calculated for a progressive loss ranging from 0 to 90%, in 10% increments, following:

$$GC_x = \left(1 - \frac{Gas\ lost\ (\%)_x}{100}\right) * GC_{initial}$$

The associated gas concentration (C_x) for each gas is calculated the same way, assuming no fractionation during the gas lost process. Thus:

$$C_x = \left(1 - \frac{Gas\ lost\ (\%)_x}{100}\right) * C_i$$

https://doi.org/10.5194/egusphere-2025-6204
Preprint. Discussion started: 13 January 2026

Uncertainties are propagated by applying the same calculation to the upper and lower bounds of the initial values (defined as ± 1 σ), thereby providing the uncertainty range for each gas-loss step (red envelop).

	Gas Content (mL/kg)	N2 (mol/kg)	O2 (mol/kg)	Ar (mol/kg)	CO2 (mol/kg)	CH4 (mol/kg)
GRIP	89.83	3.17E-03	7.85E-04	3.80E-05	1.34E-05	2.35E-07
+/-	3.90	1.73E-04	3.90E-05	2.11E-06	7.33E-06	2.75E-07
Camp Century	59.43	2.06E-03	5.60E-04	2.55E-05	2.29E-06	2.90E-09
+/-	2.78	1.21E-04	3.39E-05	1.48E-06	4.11E-07	4.65E-10

Table B1: Starting point values for the ideal gas loss scenario for GRIP and Camp Century, including 1σ uncertainties. Values correspond to the samples with the highest measured gas content.

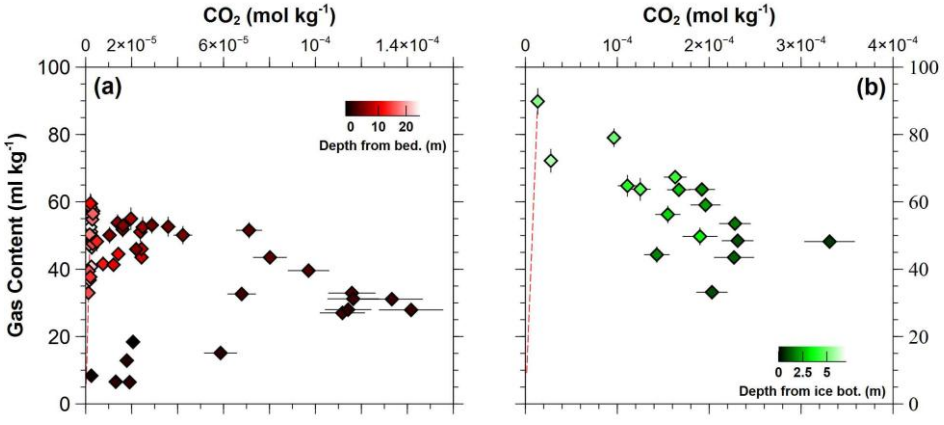

Figure B4: Variations in the concentrations of CO_2 concentration (mol kg^{-1}) as a function of gas content (ml kg^{-1}). gas content in (a) Camp Century and (b) GRIP ice cores. The colour gradients represent the depth of measurement, with lighter points indicating debris free ice above the debris-rich section.

https://doi.org/10.5194/egusphere-2025-6204
Preprint. Discussion started: 13 January 2026

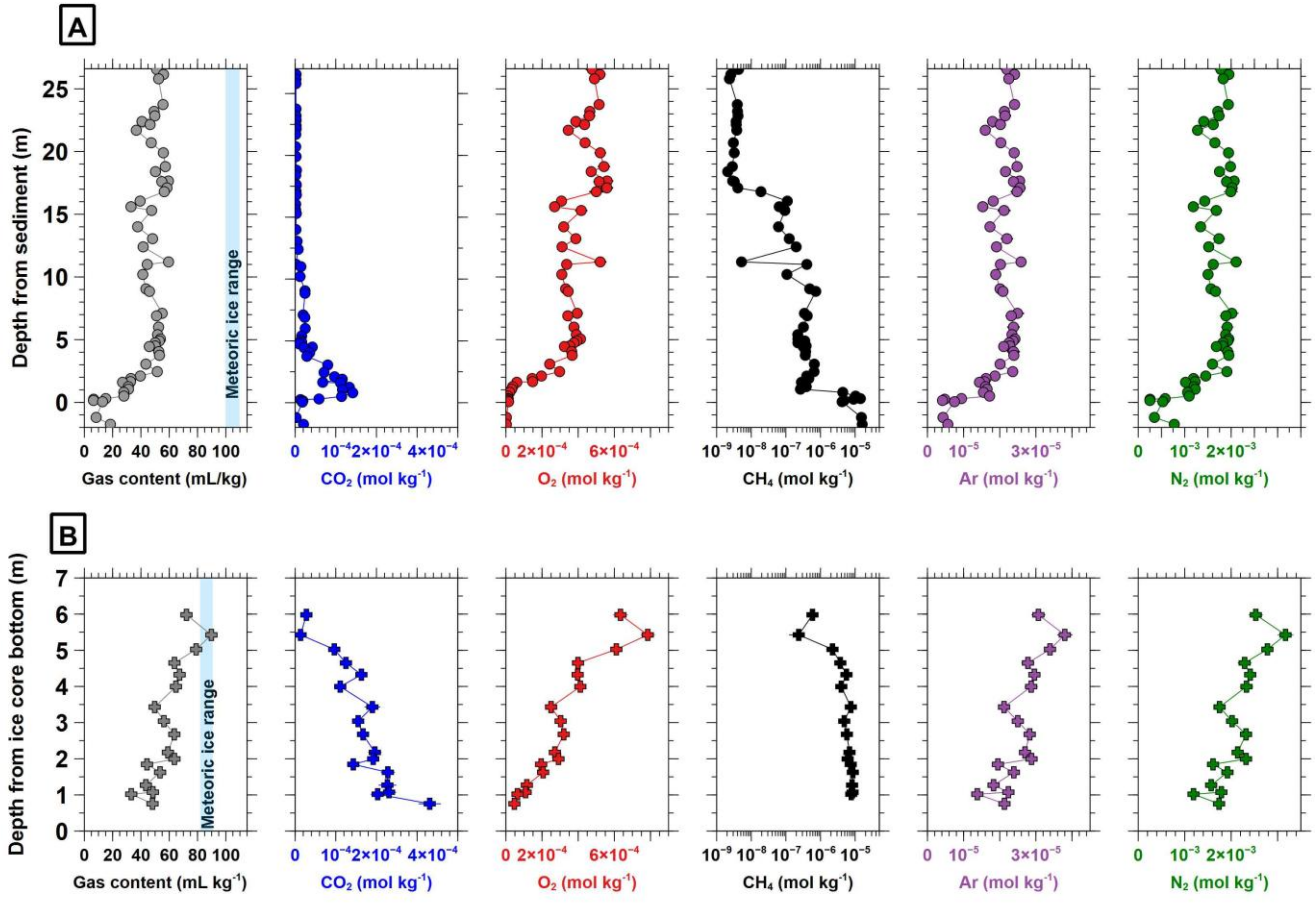

Figure B5: Gas content (in ml kg^{-1}) and gas concentration of ice (in mol kg^{-1}) in basal section of (A) Camp Century and (B) GRIP in mol kg^{-1} of ice. Note that CH_4 is in log scale.

Data availability

Water isotopes: https://doi.pangaea.de/10.1594/PANGAEA.983903

Gas measurements: https://doi.org/10.5281/zenodo.17937431

https://doi.org/10.5194/egusphere-2025-6204
Preprint. Discussion started: 13 January 2026

Author contribution

LA, FF and JLT designed the study. PHB, DDJ, JPS, JLT and FF sampled the cores; LA and SE performed the gases measurements; LA and VG performed the water isotopic measurements; CL and CK performed the DNA measurements and analysis; LA, FF and JLT wrote the manuscript draft; All authors contributed to the interpretation of the data and preparation of the final manuscript. PB, TB, CM and TR reviewed and edited the manuscript.

Competing interests

Some authors are members of the editorial board of Climate of the Past for the special issue "The Camp Century ice and sediment core: new science from a 1966 core that touched the base of the Greenland ice sheet (CP/TC inter-journal SI)".

Special issue statement

This article is part of the special issue "The Camp Century ice and sediment core: new science from a 1966 core that touched the base of the Greenland ice sheet". It is not associated with a conference.

Acknowledgements

This publication was generated in the frame of the DEEPICE project and the Green2Ice project. We thank all those who contributed to logistics, drill development and operations, field processing and analysis, and the storage and curation of the GRIP and Camp Century ice cores. In addition, we thank Julie Malaise for her contribution to debris content measurements.

Financial support

This research has been supported by the European Research Council through the European Union Horizon 2020 research and innovation programme Marie Skłodowska-Curie Actions (grant no. 955750) and through the European Research Council under the Green2Ice Synergy project was also funded by the European Union (ERC, Green2Ice, grant no. 101072180). Additional fundings were provided by the FNRS-FRS (National Fund for Scientific Research) for the AEROBIC project (grant no. CDR.J.0080.22) and the Subventions Jaumotte-Demoulin for the GENIAL project. Bierman is supported by US National Science Foundation Office of Polar Programs (grant no. EAR-OPP-2114629), the Division of Earth Sciences (grant no. NSF-EAR-1735676 and 2300560).

https://doi.org/10.5194/egusphere-2025-6204
Preprint. Discussion started: 13 January 2026

References

Adnew, G. A., Röckmann, T., Blunier, T., Jørgensen, C. J., Sapper, S. E., van der Veen, C., Sivan, M., Popa, M. E., and Christiansen, J. R.: Clumped isotope measurements reveal aerobic oxidation of methane below the Greenland ice sheet, Geochim. Cosmochim. Acta, 389, 249–264, https://doi.org/10.1016/j.gca.2024.11.009, 2025.

Ahn, J., Headly, M., Wahlen, M., Brook, E. J., Mayewski, P. A., and Taylor, K. C.: CO_2 diffusion in polar ice: observations from naturally formed CO_2 spikes in the Siple Dome (Antarctica) ice core, J. Glaciol., 54, 685–695, https://doi.org/10.3189/002214308786570764, 2008.

Alley, R. B., Gow, A. J., Meese, D. A., Fitzpatrick, J. J., Waddington, E. D., and Bolzan, J. F.: Grain-scale processes, folding, and stratigraphic disturbance in the GISP2 ice core, J. Geophys. Res. Oceans, 102, 26819–26830, https://doi.org/10.1029/96JC03836, 1997.

Anthony, C.: The quinoprotein dehydrogenases for methanol and glucose, Arch. Biochem. Biophys., 428, 2–9, https://doi.org/10.1016/j.abb.2004.03.038, 2004.

Ardoin, L., Tison, J.-L., Blard, P.-H., Dahl-Jensen, D., Steffensen, J. P., and Fripiat, F.: Gas measurements (N2, O2, Ar, CO2, CH4) of Camp Century and GRIP debris-rich ice., https://doi.org/10.5281/zenodo.17937431, 2025a.

Ardoin, L., Gkinis, V., Fripiat, F., Tison, J.-L., Dahl-Jensen, D., and Steffensen, J. P.: Water isotopic measurements of the basal ice layers of the 1966 Camp Century ice core (Greenland), 2025b.

Bender, M. L., Burgess, E., Alley, R. B., Barnett, B., and Clow, G. D.: On the nature of the dirty ice at the bottom of the GISP2 ice core, Earth Planet. Sci. Lett., 299, 466–473, https://doi.org/10.1016/j.epsl.2010.09.033, 2010.

Bereiter, B., Eggleston, S., Schmitt, J., Nehrbass-Ahles, C., Stocker, T. F., Fischer, H., Kipfstuhl, S., and Chappellaz, J.: Revision of the EPICA Dome C CO_2 record from 800 to 600 kyr before present: Analytical bias in the EDC CO2 record, Geophys. Res. Lett., 42, 542–549, https://doi.org/10.1002/2014GL061957, 2015.

Bierman, P. R., Corbett, L. B., Graly, J. A., Neumann, T. A., Lini, A., Crosby, B. T., and Rood, D. H.: Preservation of a Preglacial Landscape Under the Center of the Greenland Ice Sheet, Science, https://doi.org/10.1126/science.1249047, 2014.

Bierman, P. R., Christ, A. J., Collins, C. M., Mastro, H. M., Souza, J., Blard, P.-H., Brachfeld, S., Courville, Z. R., Rittenour, T. M., Thomas, E. K., Tison, J.-L., and Fripiat, F.: Scientific history, sampling approach, and physical characterization of the Camp Century subglacial material, a rare archive from beneath the Greenland Ice Sheet, The Cryosphere, 18, 4029–4052, https://doi.org/10.5194/tc-18-4029-2024, 2024.

Boetius, A., Ravenschlag, K., Schubert, C. J., Rickert, D., Widdel, F., Gieseke, A., Amann, R., Jørgensen, B. B., Witte, U., and Pfannkuche, O.: A marine microbial consortium apparently mediating anaerobic oxidation of methane, Nature, 407, 623–626, https://doi.org/10.1038/35036572, 2000.

Boyd, E. S., Skidmore, M., Mitchell, A. C., Bakermans, C., and Peters, J. W.: Methanogenesis in subglacial sediments, Environ. Microbiol. Rep., 2, 685–692, https://doi.org/10.1111/j.1758-2229.2010.00162.x, 2010.

Buchfink, B., Xie, C., and Huson, D. H.: Fast and sensitive protein alignment using DIAMOND, Nat. Methods, 12, 59–60, https://doi.org/10.1038/nmeth.3176, 2015.

Budd, W. F.: Ice Flow Over Bedrock Perturbations, J. Glaciol., 9, 29–48, https://doi.org/10.3189/S0022143000026770, 1970.

https://doi.org/10.5194/egusphere-2025-6204
Preprint. Discussion started: 13 January 2026

Burns, R., Wynn, P. M., Barker, P., McNamara, N., Oakley, S., Ostle, N., Stott, A. W., Tuffen, H., Zhou, Z., Tweed, F. S., Chesler, A., and Stuart, M.: Direct isotopic evidence of biogenic methane production and efflux from beneath a temperate glacier, Sci. Rep., 8, 17118, https://doi.org/10.1038/s41598-018-35253-2, 2018.

Capron, E., Landais, A., Chappellaz, J., Schilt, A., Buiron, D., Dahl-Jensen, D., Johnsen, S. J., Jouzel, J., Lemieux-Dudon, B., Loulergue, L., Leuenberger, M., Masson-Delmotte, V., Meyer, H., Oerter, H., and Stenni, B.: Millennial and sub-millennial scale climatic variations recorded in polar ice cores over the last glacial period, Clim. Past, 6, 345–365, https://doi.org/10.5194/cp-6-345-2010, 2010.

Chappellaz, J., Brook, E., Blunier, T., and Malaizé, B.: CH4 and δ18O of O2 records from Antarctic and Greenland ice: A clue for stratigraphic disturbance in the bottom part of the Greenland Ice Core Project and the Greenland Ice Sheet Project 2 ice cores, J. Geophys. Res. Oceans, 102, 26547–26557, https://doi.org/10.1029/97JC00164, 1997.

Chistoserdova, L.: Modularity of methylotrophy, revisited, Environ. Microbiol., 13, 2603–2622, https://doi.org/10.1111/j.1462-2920.2011.02464.x, 2011.

Christ, A. J., Bierman, P. R., Schaefer, J. M., Dahl-Jensen, D., Steffensen, J. P., Corbett, L. B., Peteet, D. M., Thomas, E. K., Steig, E. J., Rittenour, T. M., Tison, J.-L., Blard, P.-H., Perdrial, N., Dethier, D. P., Lini, A., Hidy, A. J., Caffee, M. W., and Southon, J.: A multimillion-year-old record of Greenland vegetation and glacial history preserved in sediment beneath 1.4 km of ice at Camp Century, Proc. Natl. Acad. Sci., 118, e2021442118, https://doi.org/10.1073/pnas.2021442118, 2021.

Christ, A. J., Rittenour, T. M., Bierman, P. R., Keisling, B. A., Knutz, P. C., Thomsen, T. B., Keulen, N., Fosdick, J. C., Hemming, S. R., Tison, J.-L., Blard, P.-H., Steffensen, J. P., Caffee, M. W., Corbett, L. B., Dahl-Jensen, D., Dethier, D. P., Hidy, A. J., Perdrial, N., Peteet, D. M., Steig, E. J., and Thomas, E. K.: Deglaciation of northwestern Greenland during Marine Isotope Stage 11, Science, 381, 330–335, https://doi.org/10.1126/science.ade4248, 2023.

Christiansen, J. R., Röckmann, T., Popa, M. E., Sapart, C. J., and Jørgensen, C. J.: Carbon Emissions From the Edge of the Greenland Ice Sheet Reveal Subglacial Processes of Methane and Carbon Dioxide Turnover, J. Geophys. Res. Biogeosciences, 126, e2021JG006308, https://doi.org/10.1029/2021JG006308, 2021.

Coleman, D. D., Risatti, J. B., and Schoell, M.: Fractionation of carbon and hydrogen isotopes by methane-oxidizing bacteria, Geochim. Cosmochim. Acta, 45, 1033–1037, https://doi.org/10.1016/0016-7037(81)90129-0, 1981.

Collins, C. M., Perdrial, N., Blard, P.-H., Keulen, N., Mahaney, W. C., Mastro, H., Souza, J., Rizzo, D. M., Marrocchi, Y., Knutz, P. C., and Bierman, P. R.: Characterization of the 1966 Camp Century Sub-Glacial Core: A Multiscale Analysis, https://doi.org/10.5194/egusphere-2024-2194, 18 July 2024.

Cuffey, K. M. and Paterson, W. S. B.: The Physics of Glaciers, Academic Press, 721 pp., 2010.

Dansgaard, W., Johnsen, S. J., Clausen, H. B., Dahl-Jensen, D., Gundestrup, N. S., Hammer, C. U., Hvidberg, C. S., Steffensen, J. P., Sveinbjörnsdottir, A. E., Jouzel, J., and Bond, G.: Evidence for general instability of past climate from a 250-kyr ice-core record, Nature, 364, 218–220, https://doi.org/10.1038/364218a0, 1993.

Dieser, M.: Molecular and biogeochemical evidence for methane cycling beneath the western margin of the Greenland Ice Sheet, ISME J., 2014.

Doyle, S. M., Montross, S. N., Skidmore, M. L., and Christner, B. C.: Characterizing Microbial Diversity and the Potential for Metabolic Function at −15 °C in the Basal Ice of Taylor Glacier, Antarctica, Biology, 2, 1034–1053, https://doi.org/10.3390/biology2031034, 2013.

https://doi.org/10.5194/egusphere-2025-6204
Preprint. Discussion started: 13 January 2026

Egger, M., Rasigraf, O., Sapart, C. J., Jilbert, T., Jetten, M. S. M., Röckmann, T., van der Veen, C., Bândă, N., Kartal, B., Ettwig, K. F., and Slomp, C. P.: Iron-Mediated Anaerobic Oxidation of Methane in Brackish Coastal Sediments, Environ. Sci. Technol., 49, 277–283, https://doi.org/10.1021/es503663z, 2015.

Eren, A. M., Kiefl, E., Shaiber, A., Veseli, I., Miller, S. E., Schechter, M. S., Fink, I., Pan, J. N., Yousef, M., Fogarty, E. C., Trigodet, F., Watson, A. R., Esen, Ö. C., Moore, R. M., Clayssen, Q., Lee, M. D., Kivenson, V., Graham, E. D., Merrill, B. D., Karkman, A., Blankenberg, D., Eppley, J. M., Sjödin, A., Scott, J. J., Vázquez-Campos, X., McKay, L. J., McDaniel, E. A., Stevens, S. L. R., Anderson, R. E., Fuessel, J., Fernandez-Guerra, A., Maignien, L., Delmont, T. O., and Willis, A. D.: Community-led, integrated, reproducible multi-omics with anvi'o, Nat. Microbiol., 6, 3–6, https://doi.org/10.1038/s41564-020-00834-3, 2021.

Ettwig, K. F., Butler, M. K., Le Paslier, D., Pelletier, E., Mangenot, S., Kuypers, M. M. M., Schreiber, F., Dutilh, B. E., Zedelius, J., de Beer, D., Gloerich, J., Wessels, H. J. C. T., van Alen, T., Luesken, F., Wu, M. L., van de Pas-Schoonen, K. T., Op den Camp, H. J. M., Janssen-Megens, E. M., Francoijs, K.-J., Stunnenberg, H., Weissenbach, J., Jetten, M. S. M., and Strous, M.: Nitrite-driven anaerobic methane oxidation by oxygenic bacteria, Nature, 464, 543–548, https://doi.org/10.1038/nature08883, 2010.

Flückiger, J., Monnin, E., Stauffer, B., Schwander, J., Stocker, T. F., Chappellaz, J., Raynaud, D., and Barnola, J.-M.: High-resolution Holocene N $_2$ O ice core record and its relationship with CH $_4$ and CO $_2$: HIGH-RESOLUTION HOLOCENE N $_2$ O ICE CORE RECORD, Glob. Biogeochem. Cycles, 16, 10-1-10–8, https://doi.org/10.1029/2001GB001417, 2002.

Foght, J., Aislabie, J., Turner, S., Brown, C. E., Ryburn, J., Saul, D. J., and Lawson, W.: Culturable Bacteria in Subglacial Sediments and Ice from Two Southern Hemisphere Glaciers, Microb. Ecol., 47, https://doi.org/10.1007/s00248-003-1036-5, 2004.

Gautam, A., Zeng, W., and Huson, D. H.: MeganServer: facilitating interactive access to metagenomic data on a server, Bioinformatics, 39, btad105, https://doi.org/10.1093/bioinformatics/btad105, 2023.

Gkinis, V., Vinther, B. M., Popp, T. J., Quistgaard, T., Faber, A.-K., Holme, C. T., Jensen, C.-M., Lanzky, M., Lütt, A.-M., Mandrakis, V., Ørum, N.-O., Pedersen, A.-S., Vaxevani, N., Weng, Y., Capron, E., Dahl-Jensen, D., Hörhold, M., Jones, T. R., Jouzel, J., Landais, A., Masson-Delmotte, V., Oerter, H., Rasmussen, S. O., Steen-Larsen, H. C., Steffensen, J.-P., Sveinbjörnsdóttir, Á.-E., Svensson, A., Vaughn, B., and White, J. W. C.: A 120,000-year long climate record from a NW-Greenland deep ice core at ultra-high resolution, Sci. Data, 8, 141, https://doi.org/10.1038/s41597-021-00916-9, 2021.

Goossens, T., Sapart, C. J., Dahl-Jensen, D., Popp, T., El Amri, S., and Tison, J.-L.: A comprehensive interpretation of the NEEM basal ice build-up using a multi-parametric approach, The Cryosphere, 10, 553–567, https://doi.org/10.5194/tc-10-553-2016, 2016.

Hakemian, A. S. and Rosenzweig, A. C.: The Biochemistry of Methane Oxidation, Annu. Rev. Biochem., 76, 223–241, https://doi.org/10.1146/annurev.biochem.76.061505.175355, 2007.

Hansen, L. and Langway, C. C.: Deep Core Drilling in Ice and Core Analysis at Camp Century, Greenland, 1961-1966, 1966.

Hanson, R. S. and Hanson, T. E.: Methanotrophic bacteria, Microbiol. Rev., 60, 439–471, https://doi.org/10.1128/mr.60.2.439-471.1996, 1996.

Herron, S., Hoar, and Langway, C. C.: The Debris-Laden Ice at the Bottom of the Greenland Ice Sheet, J. Glaciol., 23, 193–207, https://doi.org/10.3189/S002214300002983X, 1979.

https://doi.org/10.5194/egusphere-2025-6204
Preprint. Discussion started: 13 January 2026

Herron, S. L. and Langway, C. C.: A Comparison of Ice Fabrics and Textures at Camp Century, Greenland and Byrd Station, Antarctica, Ann. Glaciol., 3, 118–124, https://doi.org/10.3189/S0260305500002639, 1982.

Higaki, S., Oya, Y., and Makide, Y.: Emission of Methane from Stainless Steel Surface Investigated by Using Tritium as a Radioactive Tracer, Chem. Lett. - CHEM LETT, 35, 292–293, https://doi.org/10.1246/cl.2006.292, 2006.

Hubbard, B., Cook, S., and Coulson, H.: Basal ice facies: a review and unifying approach, Quat. Sci. Rev., 28, 1956–1969, https://doi.org/10.1016/j.quascirev.2009.03.005, 2009.

Huson, D. H., Beier, S., Flade, I., Górska, A., El-Hadidi, M., Mitra, S., Ruscheweyh, H.-J., and Tappu, R.: MEGAN Community Edition - Interactive Exploration and Analysis of Large-Scale Microbiome Sequencing Data, PLOS Comput. Biol., 12, e1004957, https://doi.org/10.1371/journal.pcbi.1004957, 2016.

Ikeda-Fukazawa, T., Fukumizu, K., Kawamura, K., Aoki, S., Nakazawa, T., and Hondoh, T.: Effects of molecular diffusion on trapped gas composition in polar ice cores, Earth Planet. Sci. Lett., 229, 183–192, https://doi.org/10.1016/j.epsl.2004.11.011, 2005.

Kinnaman, F. S., Valentine, D. L., and Tyler, S. C.: Carbon and hydrogen isotope fractionation associated with the aerobic microbial oxidation of methane, ethane, propane and butane, Geochim. Cosmochim. Acta, 71, 271–283, https://doi.org/10.1016/j.gca.2006.09.007, 2007.

Knight, P. G.: The basal ice layer of glaciers and ice sheets, Quat. Sci. Rev., 16, 975–993, https://doi.org/10.1016/S0277-3791(97)00033-4, 1997.

Krüger, M., Meyerdierks, A., Glöckner, F. O., Amann, R., Widdel, F., Kube, M., Reinhardt, R., Kahnt, J., Böcher, R., Thauer, R. K., and Shima, S.: A conspicuous nickel protein in microbial mats that oxidize methane anaerobically, Nature, 426, 878–881, https://doi.org/10.1038/nature02207, 2003.

Lamarche-Gagnon, G., Wadham, J. L., Sherwood Lollar, B., Arndt, S., Fietzek, P., Beaton, A. D., Tedstone, A. J., Telling, J., Bagshaw, E. A., Hawkings, J. R., Kohler, T. J., Zarsky, J. D., Mowlem, M. C., Anesio, A. M., and Stibal, M.: Greenland melt drives continuous export of methane from the ice-sheet bed, Nature, 565, 73–77, https://doi.org/10.1038/s41586-018-0800-0, 2019.

Landais, A., Masson-Delmotte, V., Jouzel, J., Raynaud, D., Johnsen, S., Huber, C., Leuenberger, M., Schwander, J., and Minster, B.: The glacial inception as recorded in the NorthGRIP Greenland ice core: timing, structure and associated abrupt temperature changes, Clim. Dyn., 26, 273–284, https://doi.org/10.1007/s00382-005-0063-y, 2006.

Langmead, B. and Salzberg, S. L.: Fast gapped-read alignment with Bowtie 2, Nat. Methods, 9, 357–359, https://doi.org/10.1038/nmeth.1923, 2012.

Lanoil, B., Skidmore, M., Priscu, J. C., Han, S., Foo, W., Vogel, S. W., Tulaczyk, S., and Engelhardt, H.: Bacteria beneath the West Antarctic Ice Sheet, Environ. Microbiol., 11, 609–615, https://doi.org/10.1111/j.1462-2920.2008.01831.x, 2009.

Lauritzen, M. L., Solgaard, A., Rathmann, N. M., Vinther, B. M., Grindsted, A., Noël, B., Aðalgeirsdóttir, G., and Schøtt Hvidberg, C.: Modeled Greenland Ice Sheet evolution constrained by ice-core-derived Holocene elevation histories, The Cryosphere, 19, 3599–3622, https://doi.org/10.5194/tc-19-3599-2025, 2025.

Li, D., Liu, C.-M., Luo, R., Sadakane, K., and Lam, T.-W.: MEGAHIT: an ultra-fast single-node solution for large and complex metagenomics assembly via succinct de Bruijn graph, Bioinformatics, 31, 1674–1676, https://doi.org/10.1093/bioinformatics/btv033, 2015.

https://doi.org/10.5194/egusphere-2025-6204
Preprint. Discussion started: 13 January 2026

MacGregor, J. A., Fahnestock, M. A., Catania, G. A., Aschwanden, A., Clow, G. D., Colgan, W. T., Gogineni, S. P., Morlighem, M., Nowicki, S. M. J., Paden, J. D., Price, S. F., and Seroussi, H.: A synthesis of the basal thermal state of the Greenland Ice Sheet, J. Geophys. Res. Earth Surf., 121, 1328–1350, https://doi.org/10.1002/2015JF003803, 2016a.

MacGregor, J. A., Fahnestock, M. A., Catania, G. A., Aschwanden, A., Clow, G. D., Colgan, W. T., Gogineni, S. P., Morlighem, M., Nowicki, S. M. J., Paden, J. D., Price, S. F., and Seroussi, H.: A synthesis of the basal thermal state of the Greenland Ice Sheet, J. Geophys. Res. Earth Surf., 121, 1328–1350, https://doi.org/10.1002/2015JF003803, 2016b.

Mann, H. B. and Whitney, D. R.: On a Test of Whether one of Two Random Variables is Stochastically Larger than the Other, Ann. Math. Stat., 18, 50–60, 1947.

Marath, N. K. and Wettlaufer, J. S.: Impurity effects in thermal regelation, Soft Matter, 16, 5886–5891, https://doi.org/10.1039/D0SM00558D, 2020.

Ng, F. S. L.: Pervasive diffusion of climate signals recorded in ice-vein ionic impurities, The Cryosphere, 15, 1787–1810, https://doi.org/10.5194/tc-15-1787-2021, 2021.

Oyabu, I., Kawamura, K., Uchida, T., Fujita, S., Kitamura, K., Hirabayashi, M., Aoki, S., Morimoto, S., Nakazawa, T., Severinghaus, J. P., and Morgan, J. D.: Fractionation of O_2/N_2 and Ar/N_2 in the Antarctic ice sheet during bubble formation and bubble–clathrate hydrate transition from precise gas measurements of the Dome Fuji ice core, The Cryosphere, 15, 5529–5555, https://doi.org/10.5194/tc-15-5529-2021, 2021.

Pain, A. J., Martin, J. B., Martin, E. E., Rennermalm, Å. K., and Rahman, S.: Heterogeneous CO2 and CH4 content of glacial meltwater from the Greenland Ice Sheet and implications for subglacial carbon processes, The Cryosphere, 2021.

Raynaud, D., Delmas, R., Ascencio, J. M., and Legrand, M.: Gas Extraction From Polar Ice Cores: A Critical Issue For Studying The Evolution of Atmospheric CO2 and Ice-Sheet Surface Elevation, Ann. Glaciol., 3, 265–268, https://doi.org/10.3189/S0260305500002895, 1982.

Rempel, A.: Englacial phase changes and intergranular flow above subglacial lakes, Ann. Glaciol., 40, 191–194, https://doi.org/10.3189/172756405781813564, 2005.

Rempel, A. W., Wettlaufer, J. S., and Waddington, E. D.: Anomalous diffusion of multiple impurity species: Predicted implications for the ice core climate records, J. Geophys. Res. Solid Earth, 107, ECV 3-1-ECV 3-12, https://doi.org/10.1029/2002JB001857, 2002.

Serrano-silva, N., Sarria-guzmán, Y., Dendooven, L., and Luna-guido, M.: Methanogenesis and Methanotrophy in Soil: A Review, Pedosphere, 24, 291–307, https://doi.org/10.1016/S1002-0160(14)60016-3, 2014.

Sharp, M., Parkes, J., Cragg, B., Fairchild, I. J., Lamb, H., and Tranter, M.: Widespread bacterial populations at glacier beds and their relationship to rock weathering and carbon cycling, Geology, 27, 107, https://doi.org/10.1130/0091-7613(1999)027%253C0107:WBPAGB%253E2.3.CO;2, 1999.

Simpson, M. J. R., Milne, G. A., Huybrechts, P., and Long, A. J.: Calibrating a glaciological model of the Greenland ice sheet from the Last Glacial Maximum to present-day using field observations of relative sea level and ice extent, Quat. Sci. Rev., 28, 1631–1657, https://doi.org/10.1016/j.quascirev.2009.03.004, 2009.

Skidmore, M., Anderson, S. P., Sharp, M., Foght, J., and Lanoil, B. D.: Comparison of Microbial Community Compositions of Two Subglacial Environments Reveals a Possible Role for Microbes in Chemical Weathering Processes, Appl. Environ. Microbiol., 71, 6986–6997, https://doi.org/10.1128/AEM.71.11.6986-6997.2005, 2005.

https://doi.org/10.5194/egusphere-2025-6204
Preprint. Discussion started: 13 January 2026

Skidmore, M. L., Foght, J. M., and Sharp, M. J.: Microbial Life beneath a High Arctic Glacier, Appl. Environ. Microbiol., 66, 3214–3220, https://doi.org/10.1128/AEM.66.8.3214-3220.2000, 2000.

Souchez, R.: The buildup of the ice sheet in central Greenland, J. Geophys. Res. Oceans, 102, 26317–26323, https://doi.org/10.1029/96JC01558, 1997.

Souchez, R. and Jouzel, J.: On the Isotopic Composition in δD and δ18O of Water and Ice During Freezing, J. Glaciol., 30, 369–372, https://doi.org/10.3189/S0022143000006249, 1984.

Souchez, R., Tison, J.-L., Lorrain, R., Lemmens, M., Janssens, L., Stievenard, M., Jouzel, J., Sveinbjörnsdottir, A., and Johnsen, S. J.: Stable isotopes in the basal silty ice preserved in the Greenland Ice Sheet at summit; environmental implications, Geophys. Res. Lett., 21, 693–696, https://doi.org/10.1029/94GL00641, 1994.

Souchez, R., Lemmens, M., and Chappellaz, J.: Flow-induced mixing in the GRIP basal ice deduced from the CO2 and CH4 records, Geophys. Res. Lett., 22, 41–44, https://doi.org/10.1029/94GL02863, 1995a.

Souchez, R., Janssens, L., Lemmens, M., and Stauffer, B.: Very low oxygen concentration in basal ice from Summit, central Greenland, Geophys. Res. Lett., 22, 2001–2004, https://doi.org/10.1029/95GL01995, 1995b.

Souchez, R., Jouzel, J., Landais, A., Chappellaz, J., Lorrain, R., and Tison, J.-L.: Gas isotopes in ice reveal a vegetated central Greenland during ice sheet invasion, Geophys. Res. Lett., 33, L24503, https://doi.org/10.1029/2006GL028424, 2006.

Stibal, M., Wadham, J. L., Lis, G. P., Telling, J., Pancost, R. D., Dubnick, A., Sharp, M. J., Lawson, E. C., Butler, C. E. H., Hasan, F., Tranter, M., and Anesio, A. M.: Methanogenic potential of Arctic and Antarctic subglacial environments with contrasting organic carbon sources, Glob. Change Biol., 18, 3332–3345, https://doi.org/10.1111/j.1365-2486.2012.02763.x, 2012.

Sugden, D., Knight, P., Livesey, N., Lorrain, R., Souchez, R., Tison, J.-L., and Jouzel, J.: Evidence for two zones of debris entrainment beneath the Greenland Ice Sheet, Nature, 328, 238–241, https://doi.org/10.1038/328238a0, 1987.

Tarnocai, C., Canadell, J. G., Schuur, E. a. G., Kuhry, P., Mazhitova, G., and Zimov, S.: Soil organic carbon pools in the northern circumpolar permafrost region, Glob. Biogeochem. Cycles, 23, https://doi.org/10.1029/2008GB003327, 2009.

Tavormina, P. L., Orphan, V. J., Kalyuzhnaya, M. G., Jetten, M. S. M., and Klotz, M. G.: A novel family of functional operons encoding methane/ammonia monooxygenase-related proteins in gammaproteobacterial methanotrophs, Environ. Microbiol. Rep., 3, 91–100, https://doi.org/10.1111/j.1758-2229.2010.00192.x, 2011.

Thorsteinsson, T., Kipfstuhl, J., and Miller, H.: Textures and fabrics in the GRIP ice core, J. Geophys. Res. Oceans, 102, 26583–26599, https://doi.org/10.1029/97JC00161, 1997.

Tison, J., Souchez, R., Wolff, E. W., Moore, J. C., Legrand, M. R., and De Angelis, M.: Is a periglacial biota responsible for enhanced dielectric response in basal ice from the Greenland Ice Core Project ice core?, J. Geophys. Res. Atmospheres, 103, 18885–18894, https://doi.org/10.1029/98JD01107, 1998.

Tison, J.-L., Thorsteinsson, T., Lorrain, R. D., and Kipfstuhl, J.: Origin and development of textures and fabrics in basal ice at Summit, Central Greenland, Earth Planet. Sci. Lett., 125, 421–437, https://doi.org/10.1016/0012-821X(94)90230-5, 1994.

Tranter, M., Brown, G. H., Hodson, A. J., and Gurnell, A. M.: Hydrochemistry as an Indicator of Subglacial Drainage System Structure: A Comparison of Alpine and Sub-Polar Environments, Hydrol. Process., 10, 541–556, https://doi.org/10.1002/(SICI)1099-1085(199604)10:4%253C541::AID-HYP391%253E3.0.CO;2-9, 1996.

https://doi.org/10.5194/egusphere-2025-6204
Preprint. Discussion started: 13 January 2026

Tranter, M., Sharp, M. J., Lamb, H. R., Brown, G. H., Hubbard, B. P., and Willis, I. C.: Geochemical weathering at the bed of Haut Glacier d'Arolla, Switzerland—a new model, Hydrol. Process., 16, 959–993, https://doi.org/10.1002/hyp.309, 2002.

Trotsenko, Y. A. and Murrell, J. C.: Metabolic Aspects of Aerobic Obligate Methanotrophy⋆, in: Advances in Applied Microbiology, vol. 63, Academic Press, 183–229, https://doi.org/10.1016/S0065-2164(07)00005-6, 2008.

Tung, H. C., Price, P. B., Bramall, N. E., and Vrdoljak, G.: Microorganisms Metabolizing on Clay Grains in 3-Km-Deep Greenland Basal Ice, Astrobiology, 6, 69–86, https://doi.org/10.1089/ast.2006.6.69, 2006.

Urmann, K., Norina, E. S., Schroth, M. H., and Zeyer, J.: Methanotrophic activity in a diffusive methane/oxygen counter-gradient in an unsaturated porous medium, J. Contam. Hydrol., 94, 126–138, https://doi.org/10.1016/j.jconhyd.2007.05.006, 2007.

Vaquer-Sunyer, R. and Duarte, C. M.: Thresholds of hypoxia for marine biodiversity, Proc. Natl. Acad. Sci., 105, 15452–15457, https://doi.org/10.1073/pnas.0803833105, 2008.

Verbeke, V., Lorrain, R., Johnsen, S. J., and Tison, J.-L.: A multiple-step deformation history of basal ice from the Dye 3 (Greenland) core: new insights from the CO_2 and CH_4 content, Ann. Glaciol., 35, 231–236, https://doi.org/10.3189/172756402781817248, 2002.

Wadham, J. L., Tranter, M., Tulaczyk, S., and Sharp, M.: Subglacial methanogenesis: A potential climatic amplifier?, Glob. Biogeochem. Cycles, 22, 2007GB002951, https://doi.org/10.1029/2007GB002951, 2008.

Wadham, J. L., Hawkings, J. R., Tarasov, L., Gregoire, L. J., Spencer, R. G. M., Gutjahr, M., Ridgwell, A., and Kohfeld, K. E.: Ice sheets matter for the global carbon cycle, Nat. Commun., 10, 3567, https://doi.org/10.1038/s41467-019-11394-4, 2019.

Wagner, D., Lipski, A., Embacher, A., and Gattinger, A.: Methane fluxes in permafrost habitats of the Lena Delta: effects of microbial community structure and organic matter quality, Environ. Microbiol., 7, 1582–1592, https://doi.org/10.1111/j.1462-2920.2005.00849.x, 2005.

Weertman, J.: General theory of water flow at the base of a glacier or ice sheet, Rev. Geophys., 10, 287–333, https://doi.org/10.1029/RG010i001p00287, 1972.

Weiss, R. F., Bucher, P., Oeschger, H., and Craig, H.: Compositional variations of gases in temperate glaciers, Earth Planet. Sci. Lett., 16, 178–184, https://doi.org/10.1016/0012-821X(72)90186-0, 1972.

Weitemeyer, K. A. and Buffett, B. A.: Accumulation and release of methane from clathrates below the Laurentide and Cordilleran ice sheets, Glob. Planet. Change, 53, 176–187, https://doi.org/10.1016/j.gloplacha.2006.03.014, 2006.

Willerslev, E., Cappellini, E., Boomsma, W., Nielsen, R., Hebsgaard, M. B., Brand, T. B., Hofreiter, M., Bunce, M., Poinar, H. N., Dahl-Jensen, D., Johnsen, S., Steffensen, J. P., Bennike, O., Schwenninger, J.-L., Nathan, R., Armitage, S., de Hoog, C.-J., Alfimov, V., Christl, M., Beer, J., Muscheler, R., Barker, J., Sharp, M., Penkman, K. E. H., Haile, J., Taberlet, P., Gilbert, M. T. P., Casoli, A., Campani, E., and Collins, M. J.: Ancient Biomolecules from Deep Ice Cores Reveal a Forested Southern Greenland, Science, 317, 111–114, https://doi.org/10.1126/science.1141758, 2007.

Williams, P. A., Coates, L., Mohammed, F., Gill, R., Erskine, P. T., Coker, A., Wood, S. P., Anthony, C., and Cooper, J. B.: The atomic resolution structure of methanol dehydrogenase from Methylobacterium extorquens, Acta Crystallogr. D Biol. Crystallogr., 61, 75–79, https://doi.org/10.1107/S0907444904026964, 2005.

https://doi.org/10.5194/egusphere-2025-6204
Preprint. Discussion started: 13 January 2026

Yau, A. M., Bender, M. L., Blunier, T., and Jouzel, J.: Setting a chronology for the basal ice at Dye-3 and GRIP: Implications for the long-term stability of the Greenland Ice Sheet, Earth Planet. Sci. Lett., 451, 1–9, https://doi.org/10.1016/j.epsl.2016.06.053, 2016.

Yde, J. C., Finster, K. W., Raiswell, R., Steffensen, J. P., Heinemeier, J., Olsen, J., Gunnlaugsson, H. P., and Nielsen, O. B.: Basal ice microbiology at the margin of the Greenland ice sheet, Ann. Glaciol., 51, 71–79, https://doi.org/10.3189/172756411795931976, 2010.